Załącznik nr 3

Self-presentation

1. Name and last name: Karol Strzałkowski
2. Held diplomas and scientific degrees, place and year of their acquisition and the title of the doctoral thesis:

June 24th 2008 – a defense of doctoral thesis "Growth and photothermal and photoelectric properties of II-VI mixed crystals"

2003-2007 postgraduate study at Institute of Physics, Nicolaus Copernicus University, Semiconductor Physics Group

2003-2005 engineering study at Department of Applied Informatics, Institute of Physics, Nicolaus Copernicus University finished with Engineering degree in Informatics, title of thesis: "Program for measurements of photoconductivity in Labview environment"

2001-2003 physics course at Institute of Physics, Nicolaus Copernicus University, finished with Master degree in Physics, title of thesis: "Thermal quenching of photoluminescence of organic layers PTCDA"

1998-2001 physics course at Institute of Physics, Nicolaus Copernicus University, Torun, Poland, finished with Bachelor degree in Physics, title of thesis: "Tensometry of semiconductors"

3. Information on employment in scientific institutions:

1 February 2013 – 31 July 2013 post-doctoral stay at National R&D Institute for Isotopic and Molecular Technologies, Cluj-Napoca, Romania
1 October 2010 – present – adjunct at Institute of Physics NCU
1 March 2007 – 30 September 2010 – assistant at Institute of Physics NCU

4. Achievement indicated in accordance with the Art. 16 Item 2 of the Act of 14 March 2003 on Academic Degrees and Title and Degrees and Title in Art (Journal of Laws No. 65, item. 95 with later amendments):

As a scientific achievement resulting from the act, I point monothematic series of publications under the collective title:

Thermal properties of II-VI semiconductors.

H1. **K. Strzałkowski**, *The composition effect on the thermal and optical properties across CdZnTe crystals*, J. Phys. D: Appl. Phys. 49 (2016) 435106 – 435112.

H2. **K. Strzałkowski**, M. Streza, D. Dadarlat, A. Marasek, *Thermal characterization of II–VI binary crystals by photopyroelectric calorimetry and infrared lock-in thermography*, J. Therm. Anal. Calorim. 119 (2015) 319 – 327.

H3. **K. Strzałkowski**, M. Streza, M. Pawlak, *Lock-in thermography versus PPE calorimetry for accurate measurements of thermophysical properties of solid samples: a comparative study*, Measurement 64 (2015) 64 – 70.

H4. **K. Strzałkowski**, D. Dadarlat, M. Streza, J. Zakrzewski, *Thermal characterization of ZnBeMnSe mixed compounds by means of photopyroelectric and lock-in thermography methods*, Appl. Phys. A 119 (2015) 1165 – 1171.

H5. **K. Strzałkowski**, D. Dadarlat, M. Streza, F. Firszt, *On the optimization of experimental parameters in photopyroelectric investigation of thermal diffusivity of solids*, Thermochim. Acta 614 (2015) 232 – 238.

H6. **K. Strzałkowski**, *Effect of lattice disorder on the thermal conductivity of ZnBeSe, ZnMgSe and ZnBeMgSe crystals*, Mater. Chem. Phys. 163 (2015) 453 – 459.

H7. **K. Strzałkowski**, F. Firszt, A. Marasek, *Thermal diffusivity, effusivity and conductivity of CdMnTe mixed crystals*, Int. J. Thermophys. 35 (2014) 2140 – 2149.

H8. **K. Strzałkowski**, *Characterization of thermal properties of Cd1-x-yZnxMgySe mixed crystals by means of photopyroelectric and infrared imaging techniques*, Mater. Sci. Eng. B 184 (2014) 80 – 87.

Discussion of the scientific/artistic goal of mentioned above publications and obtained results along with a discussion of their possible application

1. Introduction

Broadband solid solutions of II-VI compounds are very interesting semiconductors for both cognitive and application reasons. Their physical properties are poorly examined mainly because of the difficult technology of their production. These materials have been used as potential light sources [1], as magnetic materials [2], as infrared, ultraviolet, *x* and gamma ray detectors [3-5], in photovoltaics [6], as ZnO-based devices [6], and in other modern optoelectronics applications. From an application point of view the very important feature of mixed ternary and quaternary crystals is the possibility of an almost constant change of the value of their energy gap and lattice constant.

For many optoelectronic devices, proper heat dissipation is critical for correct functioning. Therefore one of the most important parameters characterizing utility materials, especially materials used in electronics, is the thermal conductivity. The phenomenon of the thermal conductivity of crystals is a complex issue. Both, phonons (crystalline lattice) and free carriers can be involved in the thermal conductivity. In the case of II-VI semiconductors, the contribution from free carriers is practically negligible [8]. The key issue in the thermal conductivity is the rigidity of the crystalline lattice and the number of scattering centers of phonons and carriers. Because of the high sensitivity of the thermal conductivity to the quality of the crystalline structure, its measurement gives a straightforward information on the quality of the material being tested. In turn, the inverse of the thermal diffusivity, called the temperature equalization coefficient, is a very important parameter from the application point of view because is needed in the design and construction of semiconductor devices. Determining the thermal parameters of completely new materials is therefore very important.

All investigated crystals were obtained by modified Bridgman method in the Semiconductor Physics Group at the Institute of Physics NCU with the lead role of the author of the proposal on the basis of binary high purity compounds such as ZnSe, ZnS, ZnTe, CdSe, CdS and CdTe. The main objective was to investigate the dependence of thermal parameters on composition for individual series of ternary and quaternary crystals. Within the scope of this work, the thermal parameters of over 50 different types of mixed crystals of II-VI groups have been characterized. These were the following groups of materials: binary ZnSe, ZnTe, CdSe and CdTe, ternary: $Zn_{1-x}Mg_xSe$, $Zn_{1-x}Be_xSe$, $Cd_{1-x}Mn_xTe$, $Cd_{1-x}Zn_xTe$ and quaternary: $Cd_{1-x-y}Zn_xMg_ySe$, $Zn_{1-x-y}Be_xMn_ySe$, $Zn_{1-x-y}Be_xMg_ySe$. All of these compounds are or may be used in modern optoelectronic devices such as lasers, light emitting diodes or detectors. The photopyroelectric calorimetry (PPE) method in different experimental configuration was used in order of determining the thermal parameters of the investigated crystals [9-11]. In this way, the thermal diffusivity and the effusivity of the tested materials were determined. In order to calculate the specific heat of the test compounds, their density was determined by geometric and mass measurements. Finally, from the simply dependencies between thermal parameters, the thermal conductivity was obtained. In this way, the main purpose of the work was fulfilled, which was the complete thermal characterization of selected crystals from II-VI

group as the function of the composition. The obtained results were analyzed using model proposed by Adachi for mixed semiconductor crystals [12,13].

The PPE technique is a contact method and its main disadvantage in case of solid samples is to provide good thermal contact between the sample and the detector [14-16]. In practice, it is realized by gluing a sample to the detector with a small amount of different types of liquids. The obtained results are usually controlled by various non-contact methods. In this proposal, the author verified the obtained results using active infrared thermography with a lock-in detection [17]. Another goal of this work was to adopt the PPE method in case of II-VI semiconductors. It has been shown that the influence of the coupling layer can be minimized by appropriate modification of the experimental system and proper selection of the coupling fluid. In this way, the photopyroelectric method has been satisfactorily adopted for the thermal characterization of II-VI crystals.

2. Theoretical background of applied measurement techniques

PPE method is based on pyroelectric detection, where the sample-detector system is excited by intensity modulated radiation in two basic configurations (Fig. 1). In case where the light falls directly on the sample, we are dealing with a *back* configuration (BPPE), otherwise the configuration is called the *front* (FPPE).

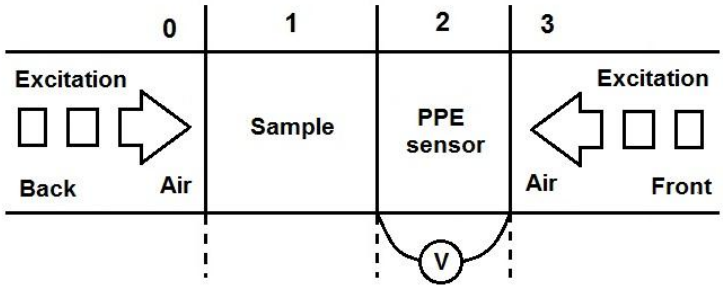

Fig. 1. Model of the experimental cell in the back and front configuration for the PPE method.

2.1 *Back* PPE configuration

In the BPPE configuration sample *s* is placed on the pyroelectric detector *p* and whole system is surrounded by air. Assuming a perfect thermal contact between the sample and the sensor and the one-dimensional model of the heat propagation through the sandwich-like system, the complex PPE signal in back configuration is given by [9-11]:

$$V = \frac{2V_0 e^{-\sigma_s L_s}}{b_{sp}+1} \frac{1-e^{-2\sigma_p L_p}}{1+R_{sp}e^{-2\sigma_p L_p}-(R_{sp}+e^{-2\sigma_p L_p})e^{-2\sigma_s L_s}} \qquad (1)$$

Where: V_0 is an instrumental factor, ij represents s and p layers of the detection cell, respectively, $R_{ij} = (b_{ij} - 1)/(b_{ij} + 1)$ is the reflection coefficient of the thermal wave at ij interface, $b_{ij} = e_i / e_j$ and e is thermal effusivity, $\sigma_i = (1+i)a_i$ is the complex diffusion

coefficient, a_i is the reciprocal of the thermal diffusion length μ_i, $a_i = 1/\mu_i$, $\mu_i = (2\alpha_i/\omega)^{1/2}$, ω is the angular modulation frequency and L_i is the thickness of the layer i. In order to eliminate the instrumental factor V_0 was eliminated applying empty sensor normalization procedure [11]. Assuming thermally thick regime for both the detector and the sample ($\mu_i << L_i$), the complex signal can be separate into amplitude (2) and phase (3):

$$\ln|V_n| = \ln\frac{2}{b_{sp}+1} - L_s\left(\frac{\omega}{2\alpha_s}\right)^{1/2} \tag{2}$$

$$\Theta_n = \Theta_0 - L_s\left(\frac{\omega}{2\alpha_s}\right)^{1/2} \tag{3}$$

The value of thermal diffusivity can be determined using both the amplitude and the phase of the pyroelectric signal. For this purpose, measurement should be made as a function of the thickness of the test specimen or modulation frequency. The first type of measurement is possible only for liquids, in the case of solids a frequency scan is performed. The thermal diffusivity values presented in this work were obtained from the slope n of the phase plot as a function of the square root of the modulation frequency. In this case the thermal diffusivity can be calculated according to the following formula:

$$\alpha_s = \frac{L_s^2\pi}{n^2} \tag{4}$$

The results obtained from the amplitude were only considered as reference, i.e.in case of large difference between amplitude and phase, the measurement was rejected as incorrect. The amplitude can be affected by external factors such as laser-intensity fluctuations and the roughness of the surface, whereas the phase is being independent on these external factors. For this reason, the thermal diffusivity was calculated according to Eq. (4).

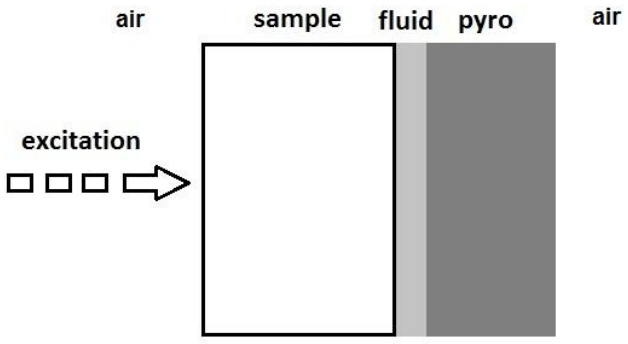

Fig. 2. The model of the five layer system.

In the above formulas, the ideal thermal contact between the detector and the test sample is assumed, omitting the effect of the coupling layer. In fact, the obtained thermal diffusivity values are always more or less affected by the additional uncertainty resulting from the need for a coupling liquid. In order to analyze this problem, numerous theoretical simulations based on the 5-layer model were performed systematically (Fig. 2). Theoretical calculations were performed on the basis of the complex equation describing such system, which was given by Salazar [15]:

$$V_n = 4\frac{1-R_s}{1-R_p}\frac{e^{-\sigma_s L_s}}{(1+b_{sf})(1+b_{fp})e^{\sigma_f L_f}+(1-b_{sf})(1-b_{fp})e^{-\sigma_f L_f}} \tag{5}$$

where: V_n is the normalized pyroelectric signal, R_i is is the optical reflection coefficient, indexes *s*, *f* and *p* refer to the opaque sample, fluid and pyroelectric sensor, respectively.

2.2 *Front* PPE configuration

In the front configuration, the excitation light falls directly on the pyroelectric, while the sample acts as a heat sink. The complex pyroelectric signal after normalization using the empty sensor procedure in this case is given by the following formula [9-11]:

$$V_n = \frac{1-e^{-\sigma_p L_p}+R_{sp}\left(e^{-2\sigma_p L_p}-e^{-\sigma_p L_p}\right)}{1+R_{sp}e^{-2\sigma_p L_p}} \tag{6}$$

Assuming a thermally thick the detector and the sample we get:

$$V_n = 1-(1+R_{sp})e^{-\sigma_p L_p} \tag{7}$$

It can be shown that in this case amplitude V_n and phase ϕ_n of the pyroelectric signal can be expressed as [11]:

$$|V_n| = \sqrt{[(1+R_{sp})e^{-a_p L_p}\sin(a_p L_p)]^2+[1-(1+R_{sp})e^{-a_p L_p}\cos(a_p L_p)]^2} \tag{8}$$

$$\phi_n = \arctan\frac{(1+R_{sp})e^{-a_p L_p}\sin(a_p L_p)}{1-(1+R_{sp})e^{-a_p L_p}\cos(a_p L_p)} \tag{9}$$

The thermal effusivity of the test sample can be obtained by matching the aforementioned theoretical relationships to the experimental points. If one knows the thermal parameters of the test sample, it is possible to determine the thermal properties of the detector itself. For the normalized phase using the empty sensor procedure the following relationship is true [11]:

$$\frac{L_p}{\mu_p} = \pi \Rightarrow \alpha_p = \frac{L_p^2 f_o}{\pi} \tag{10}$$

where f_o is the frequency, where phase is crossing zero and becomes negative. This formula enables determining the thermal diffusivity of the detector.

The disadvantage of the PPE technique especially in the *back*, but also in the *front* configuration is the need to use a liquid coupling the sample with the detector. Ensuring a perfect thermal contact in practice is very difficult task. Therefore, a thermal wave resonator cavity (TWRC) technique has been developed [11,18]. In this method, the measuring cell consists of a detector, a coupling liquid, a separator and a back layer (Fig. 3).

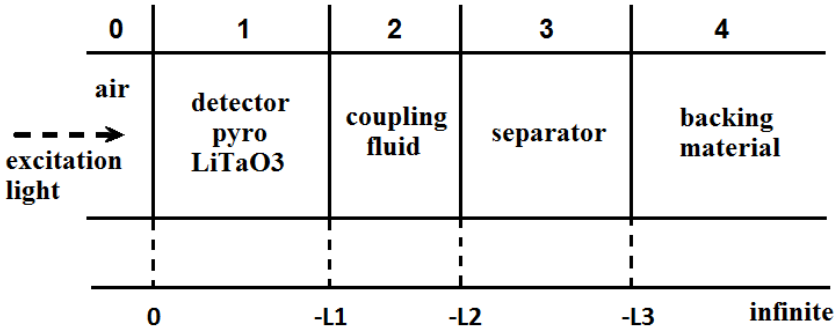

Fig. 3. The model of the cell in the front configuration for the TWRC method.

In the approximation of a one-directional heat propagation the normalized complex PPE signal is given by:

$$V_n = \frac{1-R_{21}e^{-2\sigma_1 L_1}}{1-\rho_{21}e^{-2\sigma_1 L_1}} \frac{(e^{-\sigma_1 L_1}-1)-\rho_{21}(e^{-\sigma_1 L_1}-e^{-2\sigma_1 L_1})}{(e^{-\sigma_1 L_1}-1)-R_{21}(e^{-\sigma_1 L_1}-e^{-2\sigma_1 L_1})} \tag{11}$$

where:

$$R_{21} = \frac{1-b_{21}}{1+b_{21}}$$

$$\rho_{21} = \frac{(1-b_{21})+\rho_{32}(1+b_{21})e^{-2\sigma_2 L_2}}{(1+b_{21})+\rho_{32}(1-b_{21})e^{-2\sigma_2 L_2}}$$

$$\rho_{32} = \frac{(1-b_{32})+\rho_{43}(1+b_{32})e^{-2\sigma_3 L_3}}{(1+b_{32})+\rho_{43}(1-b_{32})e^{-2\sigma_3 L_3}}$$

$$\rho_{43} = \frac{1-b_{43}}{1+b_{43}}$$

If the backing material is air and in the same time L_3 is thermally thick ($\exp(-2\sigma_3 L_3) \sim 0$) ρ_{43} does not count and ρ_{32} is reduced to (a separator layer becomes the backing): $\rho_{32} = (1 - b_{32})/(1 + b_{32})$. The main advantage of this configuration, compared to the classical frequency scanning methods, is connected with the possibility of controlling the type and the thickness variation of the coupling fluid [11]. Moreover, no additional normalization measurement is required, the normalization signal is contained in the same scanning run (thermally very thick

regime for the scanned liquid). Basically, in this configuration, one can get the thermal parameters of each layer of the detection cell (if the thermal parameters of the other layers are known). In this work one focused only on the thermal effusivity of the sample inserted as backing in the detection cell. The disadvantage of this technique compared to the standard measurement in the *front* configuration is the higher degree of complexity of the measuring system and the more time consuming measurement.

2.3 An active infrared thermography

As mentioned above, the need of using of coupling liquid in a pyroelectric method introduces the uncertainty associated with the quality of the thermal contact. For this reason, non-contact methods for the determination of the thermal diffusivity are often used to verify obtained results. In this work, an active infrared thermography with a suitable camera with built-in lock-in detection was used. The theoretical basis of thermography for determining the thermal diffusivity of the tested samples is shown below.

The heat wave equation generated by a time-periodic punctual heat source in an isotropic, homogeneous and thermally thick medium with the thermal diffusivity α, can be written as [17,19]:

$$T(x,t) = T_o e^{j(2\pi ft - kx)} \tag{12}$$

where x is the thermal wave propagation direction, T_0 is the surface temperature, f is the excitation frequency, t is the time and k is the wave vector. The 1-D thermal diffusion equation is given by:

$$\alpha \frac{\partial^2 T(x,t)}{\partial x^2} = \frac{\partial T(x,t)}{\partial t} \tag{13}$$

where:

$$k = \pm(1-j)\sqrt{\frac{\pi f}{\alpha}} \tag{14}$$

For physical reasons, the thermal wave must converge at infinity, which requires:

$$k = (1-j)\sqrt{\frac{\pi f}{\alpha}} \tag{15}$$

The thermal wave can be written as follows:

$$T(x,t) = T_o e^{-\sqrt{\frac{\pi f}{\alpha}}x} e^{j\left(2\pi ft - \sqrt{\frac{\pi f}{\alpha}}x\right)} \tag{16}$$

The propagation of a plane thermal wave through a medium of the thickness x and the thermal diffusivity α, trains a phase shift $\Delta\varphi$ having the following expression:

$$\Delta\phi = -\sqrt{\frac{\pi f}{\alpha}}x = ax \tag{17}$$

where a is the slope of the phase-distance graph. The thermal diffusion length is expressed by:

$$\mu = \frac{1}{a} = \sqrt{\frac{\alpha}{\pi f}} \tag{18}$$

The thermal diffusivity of the tested sample can be calculated according to above equation.

2.4 Description of the model given by Adachi

During measurements, the thermal diffusivity and the effusivity of the investigated crystals were obtained. It is known that all thermal parameters are related to each other. The thermal diffusivity is given by a simple formula:

$$\alpha = \frac{k}{\rho C} \tag{19}$$

where: k is the thermal conductivity, ρ is density and C is specific heat capacity. On the other hand, the thermal effusivity can be expresses as:

$$e = (k\rho C)^{1/2} \tag{20}$$

Using both expressions one can eliminate ρC factor and calculate then the thermal conductivity from simply relation:

$$k = e\alpha^{1/2} \tag{21}$$

In this way, the investigated in this work samples have been characterized for their thermal properties.

In the case of II-VI semiconductors the main contribution to the thermal conductivity is related with a phonon mechanism [8]. Lattice thermal conductivity in the case of semiconductor alloys requires taking into account a contribution, which is the result of a random distribution of constituent atoms in sublattice sites. A phenomenological model of the lattice thermal conductivity for semiconductor alloys was first proposed by Abeles [24]. However, Adachi [25,12] showed that the thermal resistivity *W(x)* for ternary $A_xB_{1-x}C$ alloy can be described by simple expression:

$$W(x) = xW_{AC} + (1-x)W_{BC} + x(1-x)C_{A-B} \quad (22)$$

where: W_{AC} and W_{BC} are binary thermal resistivities and $C_{A\text{-}B}$ is a contribution arising from the lattice disorder. Eq. (22) can be easily transferred into lattice thermal conductivity *K(x)*:

$$K(x) = \frac{1}{W(x)} = \frac{1}{xW_{AC} + (1-x)W_{BC} + x(1-x)C_{A-B}} \quad (23)$$

In this work, the results obtained for the selected ternary semiconductor alloys have been analyzed within the above model.

3. Samples and experimental setup

All the crystals, which were used for the study, were grown by high pressure and high temperature modified Bridgman method [20] at the Institute of Physics NCU with the lead role of the author of the proposal. The grown processes were carried out under typical argon pressure of about 150 atm. and allowed obtaining crystals a few centimeters in length and about 1 centimeter in diameter. Such prepared crystals were next cut into about 1.5 mm thick plates. The samples after grounding were polished with fine polishing powder. The real composition of the prepared samples was determined primarily by characteristic radiation spectroscopy using the Quantax 200 spectrometer and the EDX XFlash 4010 detector. Such prepared samples were used for pyroelectric measurements. All technological processes, except composition investigation, were carried out at the Institute of Physics of the Nicolaus Copernicus University.

The pyroelectric detection system, both in the *back* and *front* configurations, consisted of a pyroelectric detector ($LiTaO_3$ crystal plates coated with chromium and gold on both surfaces), two-phase lock-in amplifier (SR830 or SR850) and an exciting laser (532 nm, 200 mW or 405 nm, 300 mW). The laser was electronically modulated via a TTL signal fed from the lock-in amplifier in the frequency range of 1 to tens of Hz. Ethylene glycol was used as a coupling liquid in the both experimental configuration. In the *back* configuration, a diaphragm was used to prevent accidental illumination of the detector by exciting radiation. In addition, the optically transparent specimens were covered with a thin layer that absorbed incident radiation. Because the blackening layer was thin and thermally highly conductive its influence on the obtained results was neglected. In the TWRC technique, an additional element of the measuring system was a motor that allowed a precise change of the thickness of the coupling fluid.

The experimental IR setup included a heat source, a waveform generator, an infrared camera and a computer for data acquisition (Fig. 4). The intensity-modulated optical stimulation was delivered by an Nd:YAG laser (Laser Quantum OPUS, with λ=532 nm and P=0.5 W). The IR camera (FLIR 7200 series, with a 256x320 pixel array of InSb detectors sensitive in the 1.5-5.1 μm wavelength range, working at a sampling frequency of 100 Hz) recorded the changes in the surface temperature of the specimens.

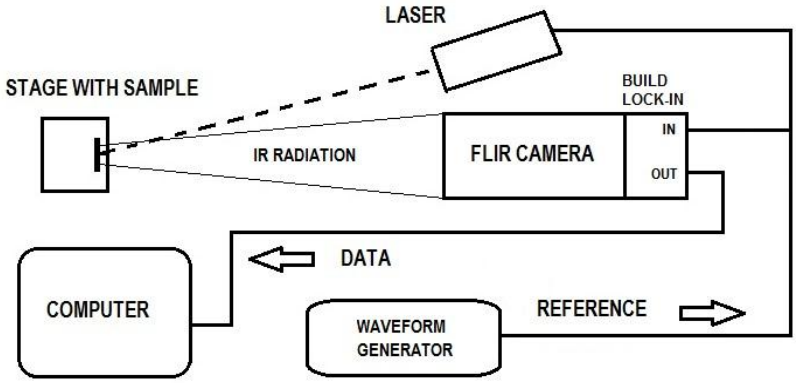

Fig. 4. Experimental setup for the lock-in thermography technique.

In the standard BPPE method, a modification was introduced to minimize the influence of the thickness of the coupling layer on the obtained thermal diffusivity values [H3, H5]. The modification consisted of pressing the test sample to the sensor by means of a disk and three identical springs acting on the disk. The schema of the altered cell in the *back* configuration is shown in Fig. 5.

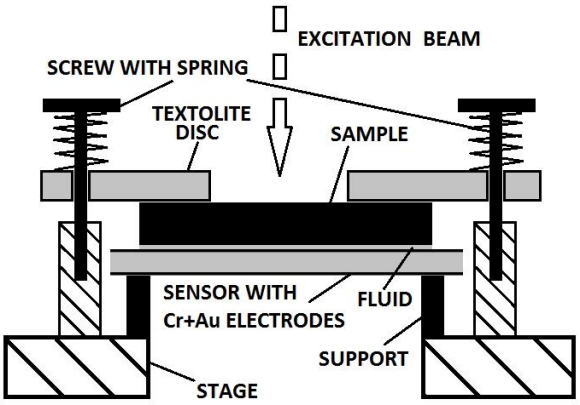

Fig. 5. Modified experimental setup for the BPPE method.

All the measurements using an infrared camera were made during a post-doctoral stay in Cluj-Napoca, Romania. Some of the photopyroelectric measurements were also made during the stay (about 30% presented in the publications). Rest of the PPE results were obtained at Institute of Physics NCU after returning from the stay using experimental setup built by the author of the proposal.

4. Discussion of the obtained results

4.1 Binary, mixed $Cd_{1-x-y}Zn_xMg_ySe$ and $Zn_{1-x-y}Be_xMn_ySe$ crystals

The thermal diffusivity of the examined binary, $Cd_{1-x-y}Zn_xMg_ySe$ and $Zn_{1-x-y}Be_xMn_ySe$ crystals was measured in BPPE configuration and by means of active infrared thermography [H2, H4, H8]. In order to compare the obtained results with the literature data, the thermal properties of selected binary II-VI crystals (ZnSe, ZnTe, CdSe and CdTe) were investigated first. In addition, glassy-like carbon GC (type G) with known material properties and a similar thermal diffusivity value compared to the studied semiconductors was used as reference sample. In the case of quaternary crystals, the methodology and measurement techniques were similar to the binary compounds. For this reason, the results of this section will be discussed on the example of binary crystals [H2].

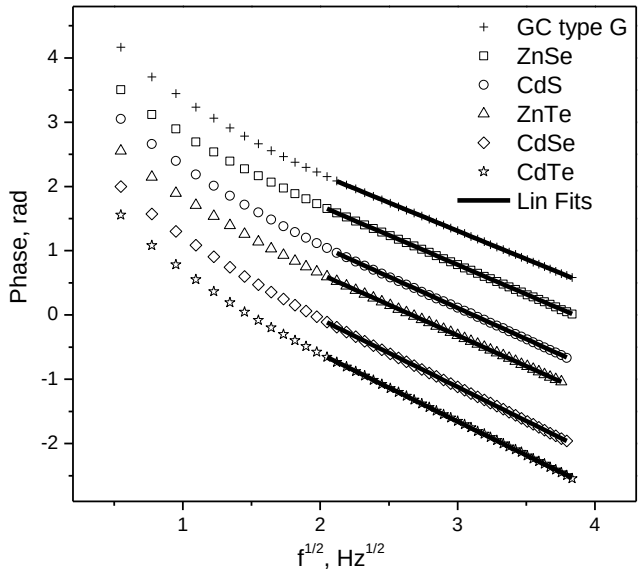

Fig. 6. The BPPE phases in radians of all investigated samples as a function of the square root of the modulation frequency, points are experimental data and lines are linear fits.

Fig. 6 presents the typical behavior of the phase as a function of the square root of the modulation frequency for binary crystals and GC sample. For low frequencies the curves exhibit a non-linear dependence due to the thermally thin regime of the sample or/and the sensor (thickness 0.5 mm). Starting from f=4 Hz, the sensor and all samples are thermally thick. In this case, according to theoretical predictions, the phase behaves linearly in the function of the square root of the modulation frequency. Consequently, linear fits have been performed in the frequency range of 4 Hz to 15 Hz, using the least square method. Thermal diffusivities were calculated according to Eq. (4).

An active infrared thermography allowed obtaining the thermal phase images of the tested samples. The phase picture obtained for the ZnSe sample (a) with the corresponding phase profiles (b and c) is shown in Fig. 7.

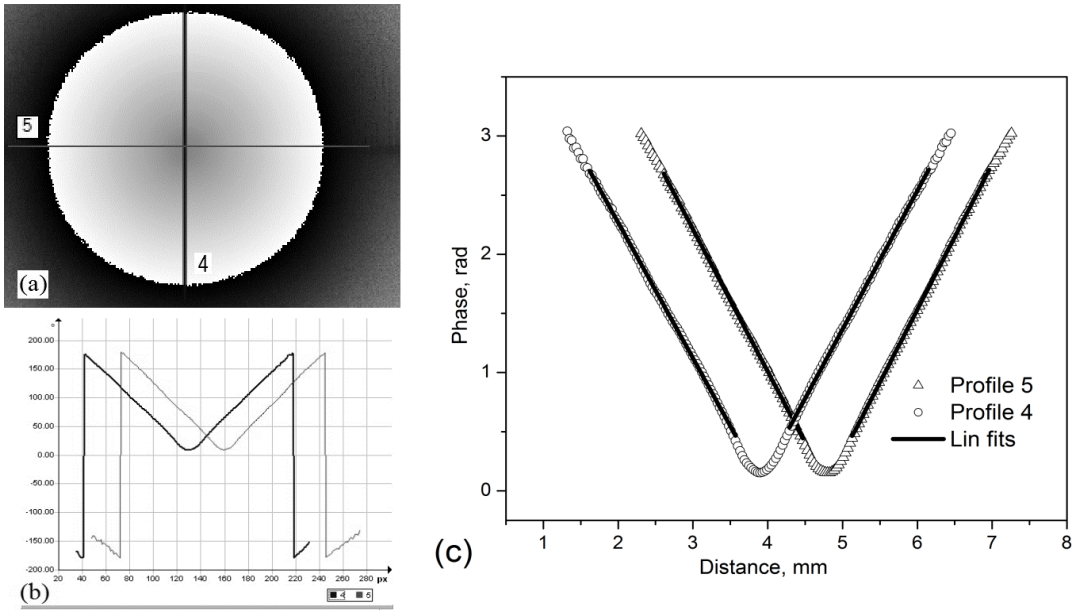

Fig. 7. Thermal image of the phase of the ZnSe (a) sample and corresponding phase profiles (b,c), circles correspond to measured data and lines are linear fits.

The impact zone of the laser is represented by the constant phase zones (plateau on the picture). The thermal wave is propagating continuously, normal to the observed object surface, symmetrically with respect to the excitation point-source. The diameter of the laser is about 150μm (1px=30μm). The thermal wave spreads on the surface over a distance of about 3 mm around the excitation source. At this distance from the excitation source, the spherical thermal wave can be approximated by a plane wave. The phase shift +180° to -180° is due to the displaying mode after lock-in detection. If such a phase shift occurs, a +360° phase-correction must be applied. Under coordinate x=60px and respectively over coordinate x=260px (see Fig. 7b, profile 5, for instance), the signal becomes noisy (meaning that the thermal wave is attenuated). The useful signal is between x=60px to x=260px. The thermal diffusivity was calculated from phase profiles, according to Eq. (18).

The thermal effusivity of the examined crystals was obtained from the TWRC method. Fig. 8 presents the results of the phase measurement as a function of the coupling fluid thickness obtained for the ZnSe crystal for two modulation frequencies, 3 and 5 Hz, together with theoretical fittings. According to the theory, two modulation frequencies 3 Hz and 5 Hz were chosen so the backing sample is thermally thick and the sensor is still thermally thin (here the thickness of the sensor was 0.2 mm). During the thickness scanning procedure thermal character of the liquid layer is changing from thermally thick to the thin one. In this way the theoretical requirements are being fulfilled. The change of the thermal character of the fluid is reflected in the course of the phase on the Fig. 8. For thermally thick regime the phase remains constant (it is used for the normalization) and goes to the minimum when the liquid becomes thermally thin. After the minimum is reached the phase increases very rapidly to its maximum. The higher value of the thermal effusivity of the backing, the wider and deeper minimum is observed as well as the difference between the minimum and maximum values in the phase is increasing.

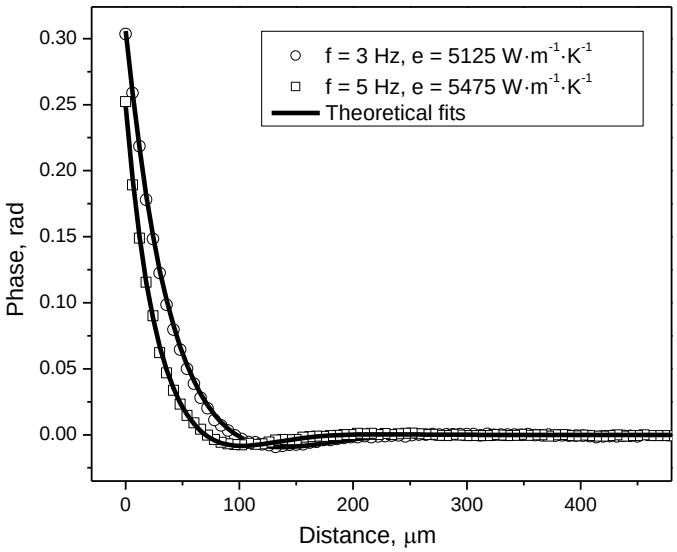

Fig. 8. The phase characteristics of the ZnSe sample measured at 3 (circles) and 5 Hz (squares), respectively with the thickness scan procedure in the front configuration, points represent experimental results and lines are theoretical fittings of the Eq. (11).

In order to obtain the sample's thermal effusivity, numerical calculations have been performed, according to Eq. (11) with two fitting parameters: the effusivity of the backing material (sample) and the value of the absolute thickness of the fluid (distance between the sample and the sensor). The least square method was applied for the fitting procedure. Thermal properties of the sensor (α=1.36 $\times 10^{-6}$ m^2s^{-1} i e=3660 $Ws^{1/2}m^{-2}K^{-1}$) and ethylene glycol (α=9.36 $\times 10^{-8}$ m^2s^{-1} i e=814 $Ws^{1/2}m^{-2}K^{-1}$) were taken from the literature [21]. The best theoretical fits and obtained values of the thermal effusivity are also displayed in Fig. 8. In this way, the thermal effusivity of the tested materials was obtained.

Table 1 contains the thermal parameters of the tested materials. The thermal conductivity was calculated using formula (21). In the case of binary and mixed $Cd_{1-x-y}Zn_xMg_ySe$ crystals, their specific heat was calculated in accordance with formula (19). For this purpose, the density of the samples was determined using the assumption of their cylindrical shape and their mass measurements by means of a precise laboratory balance.

In the case of photopyroelectric measurements and active infrared thermography, thermal diffusivity measurements for each sample were made three times. The final results presented in Table 1 were averaged over both measurement techniques. Standard deviations are shown only for the selected crystal series. The results of the thermal diffusivity obtained from BPPE were in all cases significantly lower (several percent) than in case of thermography. This observation confirms the influence of the coupling layer on the final results in PPE technique [14-16].

Tab. 1 Thermal parameters of the investigated materials, the literature data are in brackets.

Compound	Conductivity k ($W \cdot m^{-1} \cdot K^{-1}$)	Diffusivity α ($m^2 \cdot s^{-1}$)×10^{-6}	Effusivity e ($W \cdot s^{1/2} \cdot m^{-2} \cdot K^{-1}$)	Specific heat ($J \cdot kg^{-1} \cdot K^{-1}$)	Density ($kg \cdot m^{-3}$)
ZnTe	9.31 (18,[22])	7.5	3400	235.4	5275
CdSe	4.55 (9.0,[22])	3.57	2420	238.9	5401
CdTe	4.51 (7.1,[22])	4.51	2560	264.3	5501
ZnSe	13.3 (19,[22])	6.41	5300	420.92	5016.51
$Zn_{0.94}Mg_{0.06}Se$	8.96	4.51	4220	393.02	5056.05
$Zn_{0.88}Mg_{0.12}Se$	6.35	3.17	3565	396.09	5055.12
$Zn_{0.78}Mg_{0.22}Se$	3.27	1.9	2370	382.33	4497.13
$Cd_{0.24}Zn_{0.56}Mg_{0.20}Se$	2.08	1.19	1900	353.08	4926.06
$Cd_{0.41}Zn_{0.48}Mg_{0.11}Se$	2.00	1.18	1840	331.7	5103.01
$Cd_{0.40}Zn_{0.40}Mg_{0.20}Se$	1.88	1.14	1760	346.63	4765.97
$Cd_{0.44}Zn_{0.35}Mg_{0.21}Se$	1.76	1.06	1710	334.66	4966.88
$Cd_{0.31}Zn_{0.26}Mg_{0.43}Se$	1.46	1.04	1440	323.46	4375.93
$Cd_{0.55}Zn_{0.24}Mg_{0.21}Se$	1.63	1.04	1600	315.47	4969.27
$Cd_{0.62}Zn_{0.24}Mg_{0.13}Se$	1.83	1.26	1630	277.62	5223.63
$Cd_{0.37}Zn_{0.21}Mg_{0.42}Se$	1.71	1.03	1690	379.9	4387.16
$Cd_{0.45}Zn_{0.12}Mg_{0.43}Se$	1.49	0.99	1500	324.7	4646.78
$Cd_{0.66}Zn_{0.12}Mg_{0.22}Se$	1.94	1.10	1850	364.98	4832.92
$Zn_{0.90}Be_{0.05}Mn_{0.05}Se$	5.612±0.068	2.831±0.015	3322±25	-	-
$Zn_{0.79}Be_{0.05}Mn_{0.16}Se$	4.044±0.046	2.252±0.012	2692±24	-	-
$Zn_{0.67}Be_{0.05}Mn_{0.28}Se$	1.731±0.022	1.426±0.016	1454±17	-	-
$Zn_{0.84}Be_{0.11}Mn_{0.05}Se$	4.585±0.054	2.583±0.014	2853±27	-	-
$Zn_{0.77}Be_{0.18}Mn_{0.05}Se$	4.283±0.051	2.414±0.015	2760±25	-	-
$Zn_{0.69}Be_{0.26}Mn_{0.05}Se$	3.546±0.042	2.151±0.014	2415±25	-	-
GC type G	6.34 (6.3,[23])	4.15	3110	1075.1 (1050,[24])	1420

The thermal effusivities listed in Table 1 represent the average value of effusivities computed at two excitation frequencies (3 and 5 Hz, respectively). The obtained values lie within 10 % deviation of the mean. The contour maps shown in Fig. 9 represent the precision of the fit performed with Eq. (8) to the experimental data obtained for ZnSe (a) and CdSe (b) crystals respectively. The *x*-axis represents the error in the absolute value of the thickness of the coupling fluid. This absolute value is not known, only the thickness variation. The *y*-axis represents the thermal effusivity. The shape of the contour lines indicates the accuracy of the results. Contour lines extended along Ox axis indicate a good precision in thermal effusivity measurement. If they extend along Oy axis, the accuracy in the measurement of thermal effusivity is low. Circles mean similar accuracy in obtaining both thermal effusivity and location of the backing position. The accuracy of this type of investigations increases if the effusivity ratio coupling fluid/backing material goes to 1. One can see in Fig. 9 that for high backing/liquid (e_3/e_2) effusivity ratios, an accurate location of the backing material is obtained, while thermal effusivity is obtained with low precision. This is the case of ZnSe sample, where e_3/e_2 (5300/890 $W \cdot s^{1/2} \cdot m^{-2} \cdot K^{-1}$) is about 6. For CdSe sample, the ratio is two times smaller and consequently, the precision in thermal effusivity determination increases.

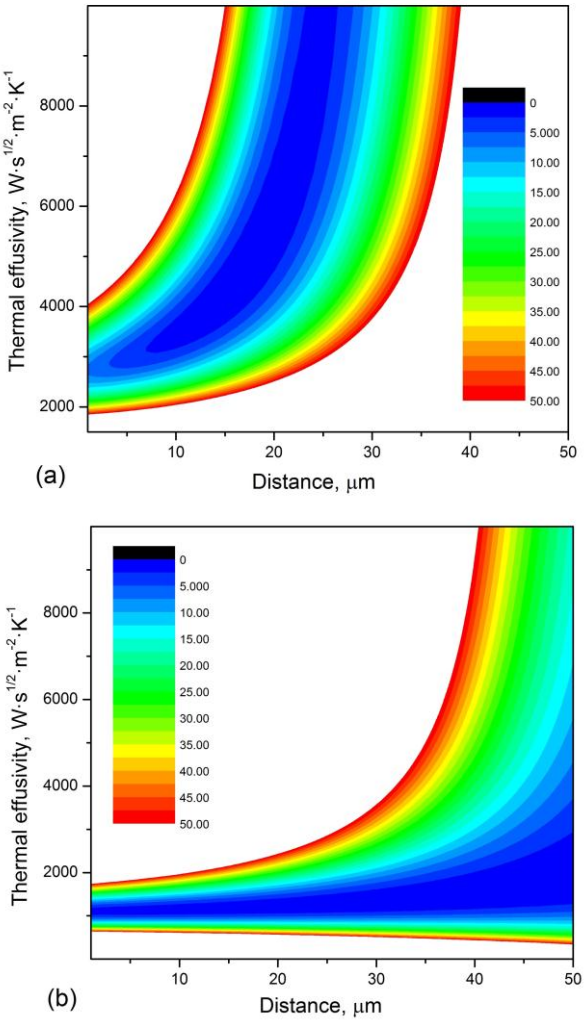

Fig. 9. Contour maps of the precision of the fittings performed with Eq. 4 to the experimental data obtained for ZnSe (a) and CdSe (b) samples respectively.

Table 1 shows that the highest values of thermal conductivity are observed for binary and mixed crystals with low concentration of added component. Adding even a few percent of the magnesium in any mixed crystal immediately causes a significant deterioration in its thermal properties. Thermal conductivity values differ between the binary ZnSe compound and the mixed crystals $Cd_{1-x-y}Zn_xMg_ySe$ or $Zn_{1-x-y}Be_xMn_ySe$ even by order of magnitude. The addition of manganese, beryllium or magnesium generates significant concentrations of various defects in these compounds, which has been confirmed experimentally [H6]. Every imperfection of the crystal lattice becomes a potential scattering center for phonons, and consequently the transport capabilities (heat, but also electrical) of such a crystal are greatly reduced. Due to the problem of the heat dissipation in electronic devices, this observation is crucial in the design of new optoelectronic devices based on any mixed compounds.

The results of the thermal conductivity for binary crystals deviate from the literature data [22]. The differences between the values obtained and the literature data observed in this case can be explained partially by a few facts/observations. Thermal properties are much more sensitive to crystal growth techniques than optical parameters. The quality of the grown

crystal, its purity, the concentration of defects are crucial here. The studied crystals were obtained by Bridgman's method, which has the disadvantage of the high electric resistivity of the resulting crystals due to the large concentration of cation vacancies. The obtained values were further influenced by the non-ideal blackening of the samples and the presence of the coupling layer between the sample and the detector.

The thermal conductivity value obtained for the GC reference sample agrees with the data given by the producer [23]. Also, the obtained specific heat value remains in good compliance with the differential scanning calorimetry [24]. By contrast, when comparing literature data for thermal diffusivity and effusivity, they are respectively under and overestimated.

Observed discrepancies between the literature and measured data prompted the author to look more closely at the used measurement techniques. The results of the optimization studies are presented in the next subsection.

4.2 Optimization of the experimental techniques

The effect of the coupling layer on the BPPE results is well known and has also been investigated by other authors [14-16]. Salazar et al. have shown that due to the presence of the coupling layer the determined thermal diffusivity of the solid sample is always underestimated [15]. This problem is particularly important for high-conductivity samples and for higher modulation frequencies (above tens of Hz). The proposed solutions of this problem are primarily based on the control of the obtained photopyroelectric results by non-contact methods, such as infrared radiometry (PTR - photothermal radiometry). The author used non-contact active thermography with the use of lock-in detection. However, the results obtained from the camera may also be subjected to an uncertainty, which is difficult to estimate accurately. Therefore, in the next work [H3], the thermal diffusivity measurements of known materials (GC, LiTaO3, CdTe and CdSe) obtained by both mentioned above methods are presented, paying particular attention to fulfill the theoretical assumptions and optimizing the experimental conditions.

To test different coupling fluids in BPPE technique, thermal diffusivity measurements were made in a standard configuration for G-type (GC) glassy-like carbon for various fluids. The obtained results are presented in Fig. 10.

The value of the thermal diffusivity of the GC sample given by other authors is in the range of $5.4\text{-}6\times10^{-6}\ m^2\cdot s^{-1}$ [16]. From the above figure, it is clear that less undervalued values were obtained for more liquid substances, with the value obtained for ethylene glycol lying within the error limits of the reference range.

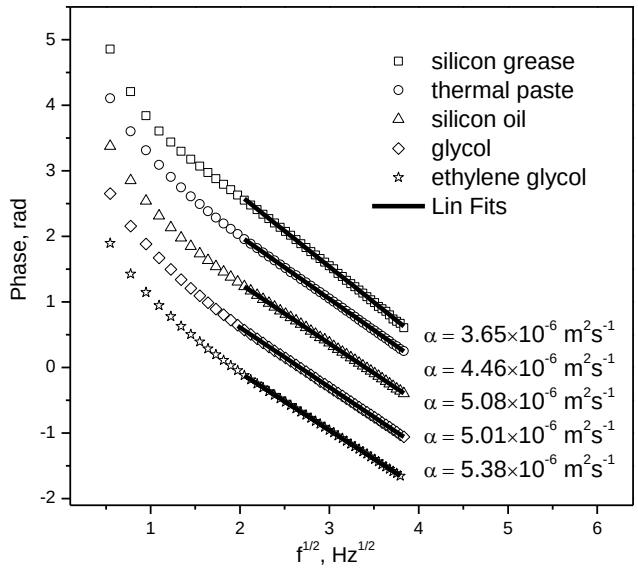

Fig. 10. Phase characteristics of glassy-like carbon for different coupling fluids as a function of the square root of the modulation frequency, points are experimental data and lines are linear fits.

In order to accurately analyze the influence of the thickness of the coupling layer on the obtained thermal diffusivity value, numerous theoretical simulations based on the five-layer model presented in Fig. 2 and equation (5) were performed [H5]. On the Fig. 11 simulations for a hypothetic solid sample with thermal diffusivity 2×10^{-6} $m^2\cdot s^{-1}$, effusivity 2000 $W\cdot s^{1/2}\cdot m^{-2}\cdot K^{-1}$ and thickness 1 mm for different thickness of the coupling fluid (ethylene glycol) are shown.

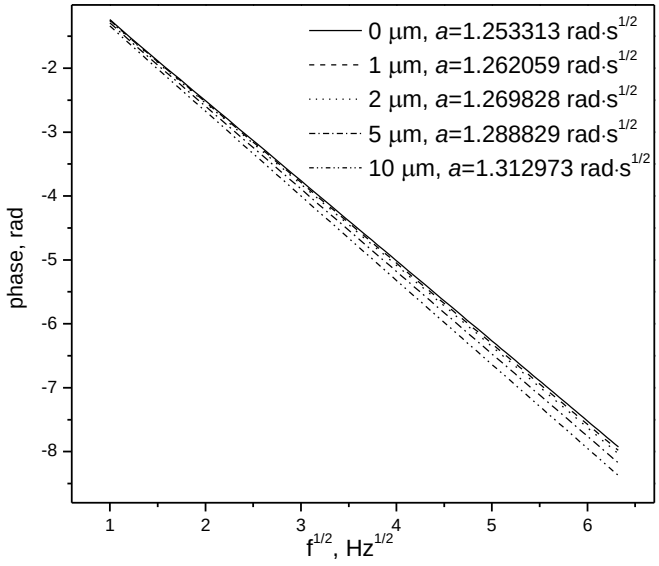

Fig. 11. Theoretical simulations of the phase of the signal for different thicknesses of the coupling fluid.

The thermal parameters of the coupling fluid and the pyroelectric sensor were taken from the literature [25]: for ethylene glycol (α_f =9.36×10^{-8} m^2·s^{-1}, e_f =890 W·s$^{1/2}$·m^{-2}·K^{-1}) and for $LiTaO_3$ (α_p =1.56×10^{-6} m^2·s^{-1}, e_p=3600 W·s$^{1/2}$·m^{-2}·K^{-1}). One can see that the slope *a* of the curve "phase vs. sqrt. (f)" increases from 1.25 to 1.31 with increasing thickness of the coupling fluid from 0 μm to 10 μm. A similar correspondence "slope of the curve phase vs. sqrt. (f)" vs. "coupling fluid thickness" was obtained in ref. [15].

Tab. 2 Relative error in thermal diffusivity evaluation, for different solid samples.

Fluid thickness (μm)	0	1	2	5	10
Error (%) for α_s = 2×10^{-6} m^2·s^{-1}	0	1.38	2.58	5.44	8.90
Error (%) for α_s = 6×10^{-6} m^2·s^{-1}	0	2.40	4.45	9.17	14.68
α_L / α_s	1/20	1/10	1/4	1/2	1/1
Error (%) for α_s = 2×10^{-6} m^2·s^{-1} and L_f=10 μm	8.68	6.82	4.87	3.70	2.77
e_L/e_s	¼	1/2	1/1	3/2	5/2
Error (%) for e_s=2000 W·s$^{1/2}$·m^{-2}·K^{-1}, L_f = 5 μm	6.29	5.25	4.47	4.39	4.75
e_L/e_s	6/1	4/1	2/1	3/2	6/5
Error (%) for e_L=6000 W·s$^{1/2}$·m^{-2}·K^{-1}, L_f = 5 μm	5.21	5.09	4.81	4.67	4.56

The results of the numerical calculation of relative error in the thermal diffusivity evaluation, by applying Eq. (5), for different sets of the parameters, are given in Table 2. The error was calculated as relative value taking into account given thermal diffusivity in comparison with value obtained for zero fluid thickness. The first three rows in Table 2 present the influence of the thickness of the coupling fluid on the value of thermal diffusivity for a solid sample with low (second row) and higher (third row) thermal diffusivity. The data presented in Table 2 support our initial statement, that the influence of the coupling medium becomes significant especially for high conductive samples. Relative error for a sample with diffusivity α_s = 6×10^{-6} m^2·s^{-1} at a liquid thickness of 10 μm was almost 15%, nearly double that of a weaker-conductive sample. The dependence of the relative error versus the thermal diffusivity ratio (α_L / α_s) is given in next two rows of Table 2. As expected, when the values of the thermal diffusivity of the coupling fluid and the sample are close, the error decreases. Last four rows in Table 2 evaluate the influence of the difference between the effusivity of the coupling fluid and that of the solid sample; this difference seems to be not so important like the thickness and the thermal diffusivity of the coupling fluid.

Based on the obtained results, it was concluded that the critical factor in BPPE contact measurement is the thickness of the coupling layer. In the case of liquids, it is easier to obtain a thin, homogeneous layer which gives good thermal contact between the sample and the detector. Ethylene glycol was chosen as the most optimal for further studies. In order to minimize the impact of the ethylene glycol layer, a simple modification to the standard measuring system was introduced, which was previously shown in Fig. 5. A comparison of experimental results obtained before and after the modification of the experimental setup on the example of CdTe sample is shown in Fig. 12. The difference in the slopes between two curves can be clearly seen, consequently the thermal diffusivity of the specimen was calculated from the slopes as 4.244±0.035×10^{-6} m^2·s^{-1} for standard configuration and as

$4.473 \pm 0.008 \times 10^{-6}$ $m^2 \cdot s^{-1}$ after applying the modification. Given thermal diffusivities were calculated as average values from three independent measurements with standard deviation as an uncertainty. One can see that thanks proposed simply solution significant reduction of the influence of the coupling fluid takes place (the final thickness of ethylene glycol is reduced). The standard deviation of the thermal diffusivity is smaller in case of modified BPPE technique indicating stable, repeatable measurement conditions.

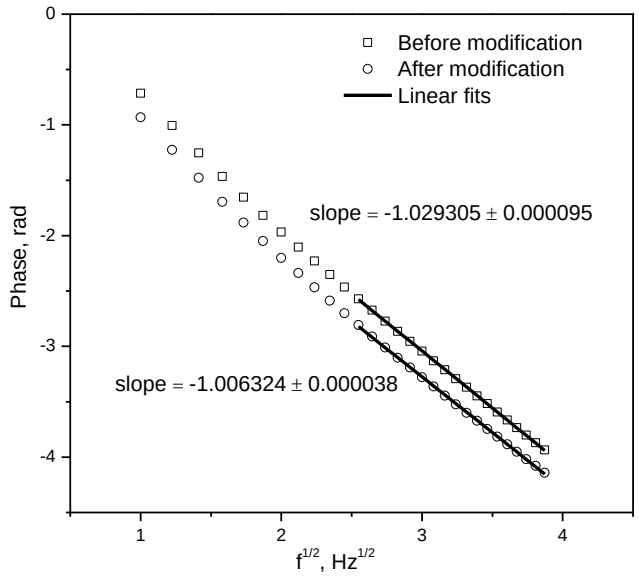

Fig. 12. Phase characteristics of CdTe sample measured before (squares) and after (circles) the modification of the experimental setup, points - experimental data and lines - linear fits.

In the course of further investigations, it was found that the values of the thermal diffusivity obtained by non-contact active infrared thermography are sensitive to the geometry of the measuring system. The test specimen should be mounted as flat-parallel to the lens of the camera. It is not easy to obtain such a setting under testing conditions of measuring system. In the case of inaccurate sample setting with respect to the camera, the slope obtained from the phase profiles (see Fig. 7 for the ZnSe crystal) may differ from each other, generating a relatively high measurement uncertainty that may be several percent of the measured value. Much larger error can generate incorrectly selected experiment conditions. According to the theory, using active thermography, one should work at the modulation frequency for which the sample is thermally thick. Failure to do so may result in an underestimation of the thermal diffusivity of up to 20-30%. Choosing the correct frequency is therefore critical, but it is not an easy task in case of new materials with unknown thermal parameters. Fig. 13 shows the results obtained for the GC sample for different modulation frequencies (0.05 - 4 Hz). For very low modulation frequency the sample is thermally thin, and convective effects cannot be ignored. The resulting thermal diffusivity value is too small; for subsequent frequencies the underestimation decreases. For 4 Hz the result is already satisfactory and falls within the range of values reported by other authors. For completely new materials to determine the approximate modulation frequency contact PPE technique can be used first.

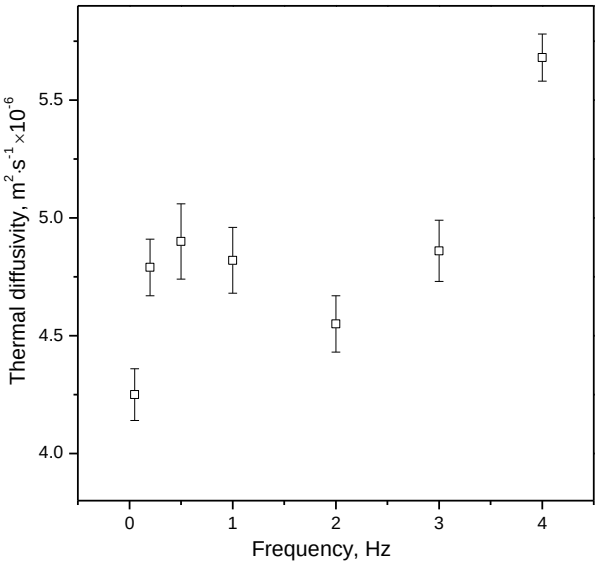

Fig. 13. Measurements of the thermal diffusivity for glassy-like carbon were performed in the frequency range of 0.05 – 4 Hz, points refer to experimental data and error bars to the standard deviation.

Results of the thermal diffusivity along with standard deviations of GC type G, CdSe, CdTe and LiTaO3 samples measured both by the modified BPPE method and by thermography are presented in Table 3.

Tab. 3 Thermal diffusivity ($m^2 \cdot s^{-1} \times 10^{-6}$) of the investigated materials

Material	PPE	Thermography	Literature
GC type G	5.378±0.021	5.601±0.135	5.4-6, [16]
CdSe	4.602±0.016	4.615±0.169	4.5, [26]
CdTe	4.473±0.008	4.485±0.135	4.78, [27]
$LiTaO_3$	1.362±0.005	1.36±0.085	1.22-1.54, [25]

Obtained thermal diffusivity values remain in good agreement with literature data given in third column and confirm an ability of applied techniques for proper thermal characterization of solid materials. For CdSe, CdTe and LiTaO3 samples there is a very good agreement between PPE and Thermography methods, obtained values lie within error bars. Some discrepancy of about 4% for glassy-like carbon can be found, however the difference is not too large. Considering standard deviation, the BPPE technique together with proposed modification is much more stable and accurate than thermography method. However, the photopyroelectric calorimetry is well established technique, in contrast to infrared lock-in thermography, which is quite new technique still under development. From the experimental point of view, infrared lock-in thermography being non-contact method, seems to be an interesting alternative because the measurements are fast and no coupling medium is required.

4.3 Compounds $Cd_{1-x}Mn_xTe$, $Zn_{1-x}Be_xSe$, $Zn_{1-x}Mg_xSe$, $Zn_{1-x-y}Be_xMg_ySe$ and $Cd_{1-x}Zn_xTe$

In this subsection, the thermal diffusivity measurements of the tested crystals were made using the modified measuring system shown in Fig. 5 and ethylene glycol as the coupling liquid. In addition, with the exception of $Cd_{1-x}Mn_xTe$ crystals, the results of the phase measurements are not expressed as a function of the square root of the modulation frequency, but of the square root of the modulation frequency multiplied by the thickness of the sample. Thanks to that the difference in the slopes of obtained curves is directly proportional to the thermal diffusivity of given specimens. The phase characteristics of the thermal diffusivity of crystals $Cd_{1-x}Zn_xTe$ are shown in Fig. 14 [H1].

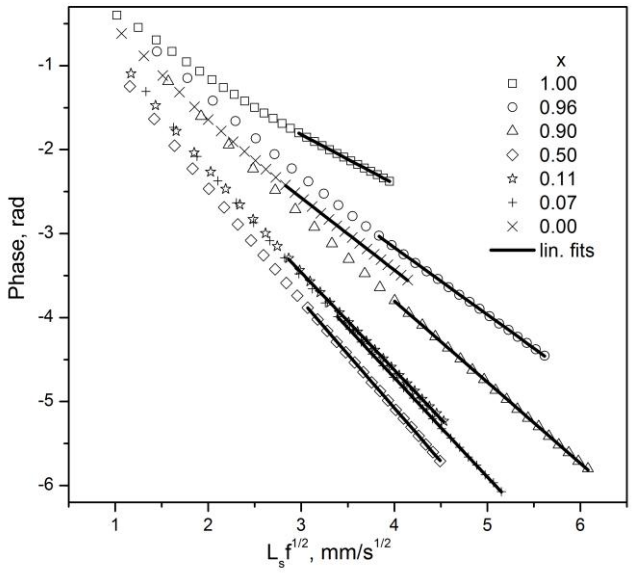

Fig. 14. Phase characteristics of $Cd_{1-x}Zn_xTe$ crystals for all zinc content, points are experimental data and lines are linear fits obtained with least square method.

Linear fits were performed in the range of frequency where both, the sample and the sensor are thermally thick. The statistical determination coefficient R^2 describing quality of fitting was better than 0.9999 for all cases. One can see in Fig. 14 that the specimens with the highest and lowest thermal diffusivity (the lowest and highest slope) are ZnTe and $Cd_{0.5}Zn_{0.5}Te$, respectively. The thermal diffusivity of investigated specimens was calculated according to Eq. (4).

Since in the TWRC method it is difficult to determine the accuracy of the obtained results and due to the complexity of the experiment, the results of the thermal effusivity measurements were obtained in the FPPE configuration. In order to calibrate and test the measuring system thermal effusivity of distilled water and ethylene glycol was measured first (Fig. 15) [H7]. The obtained results were normalized using a standardized empty sensor procedure.

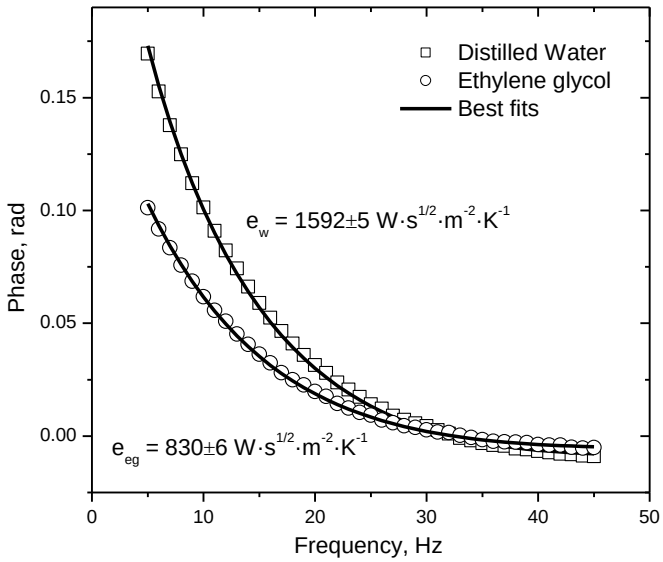

Fig. 15. Phase behavior of distilled water and ethylene glycol as a function of modulation frequency in the front configuration, points refer to measured data, lines are best fits obtained with least square method using Eq. (9).

Thermal effusivity of the water and ethylene glycol was obtained as the parameter of the fitting of the equation (9). Given values were calculated as average values from three independent measurements with standard deviation as an uncertainty. Obtained results of the thermal effusivity of water and ethylene glycol remains in good agreement with the literature data [11]. An identical measurement procedure was used for all semiconductor materials discussed in this section.

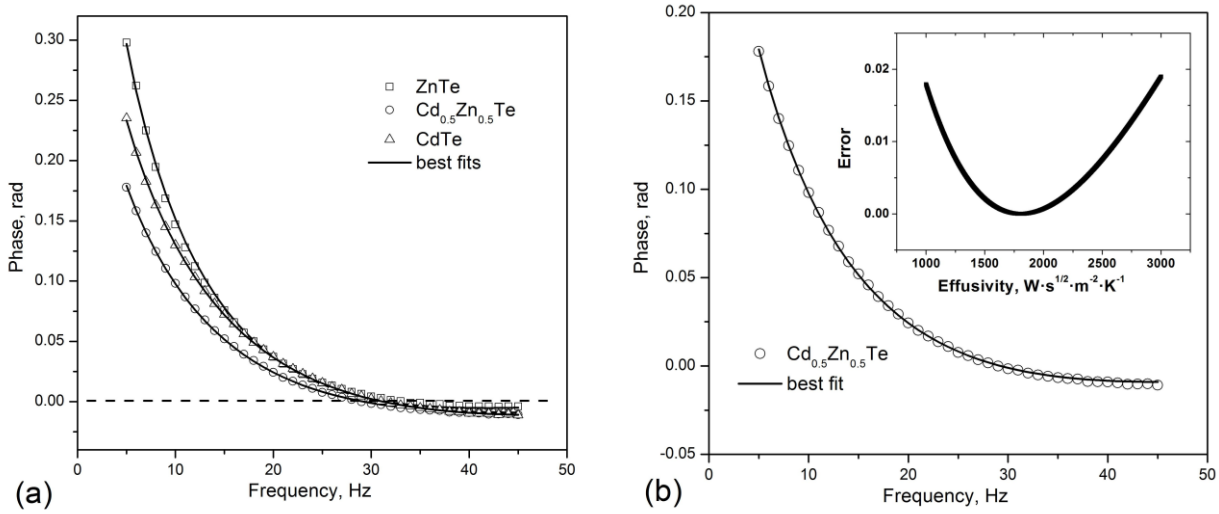

Fig. 16. Phase characteristics of selected $Cd_{1-x}Zn_xTe$ crystals as a function of modulation frequency (a), points refer to measured data, lines are best fits obtained with least square method using Eq. (9). Example fit for $Cd_{0.5}Zn_{0.5}Te$ crystal (b) and the error of the fitting procedure (see inset) is also shown.

Fig. 16 (a) and (b) present measured phase of the selected $Cd_{1-x}Zn_xTe$ crystals in the case of front configuration and example fit for $Cd_{0.5}Zn_{0.5}Te$ crystal, respectively. For clarity purposes the results for three selected crystals are only given. The determination coefficient was of the order 0.999, slightly lower than in case of back configuration. The fit of the theoretical curve to the experimental data was done with Eq. (9) applying least square method. The error of the example fitting for $Cd_{0.5}Zn_{0.5}Te$ crystal is given in the inset of the picture (b). The minimum observed in the error graph indicates the sought thermal effusivity value of the investigated sample. One can observe that all curves presented in Fig. 16 (a) cross the zero point more or less at the same modulation frequency. This observation supports the statement about proper measurement procedure. As in subsection 4.1, the thermal conductivity was calculated from the obtained results. Thermal parameters of the crystals from this section are presented in Table 4 [H1, H6, H7].

Tab. 4 Thermal parameters of the tested crystals.

Compound	Diffusivity α $(m^2 \cdot s^{-1}) \times 10^{-6}$	Effusivity e $(W \cdot s^{1/2} \cdot m^{-2} \cdot K^{-1})$	Conductivity k $(W \cdot m^{-1} \cdot K^{-1})$
CdTe	4.473±0.008	2497±17	5.280±0.042
$Cd_{0.73}Mn_{0.27}Te$	1.734±0.012	1592±8	2.096±0.017
$Cd_{0.51}Mn_{0.49}Te$	1.478±0.016	1510±15	1.836±0.028
$Cd_{0.33}Mn_{0.67}Te$	1.418±0.007	1432±7	1.705±0.0136
ZnSe	9.846±0.030	5633.3±20.2	17.676±0.09
$Zn_{0.96}Be_{0.04}Se$	4.333±0.042	3851.7±48.0	8.018±0.137
$Zn_{0.9}Be_{0.1}Se$	3.301±0.018	3333.3±10.4	6.056±0.035
$Zn_{0.83}Be_{0.17}Se$	2.691±0.013	2693.3±30.6	4.418±0.061
$Zn_{0.74}Be_{0.26}Se$	2.558±0.012	2686.7±28.4	4.297±0.055
$Zn_{0.94}Mg_{0.06}Se$	5.080±0.014	4041.7±56.2	9.109±0.139
$Zn_{0.88}Mg_{0.12}Se$	3.560±0.046	3288.3±35.1	6.204±0.106
$Zn_{0.78}Mg_{0.22}Se$	2.122±0.009	2328.3±22.5	3.392±0.040
$Zn_{0.67}Mg_{0.33}Se$	1.444±0.017	1903.3±15.3	2.287±0.032
$Zn_{0.84}Be_{0.04}Mg_{0.12}Se$	2.555±0.031	2688.3±29.3	4.297±0.073
$Zn_{0.72}Be_{0.06}Mg_{0.22}Se$	2.466±0.047	2523.3±27.5	3.962±0.081
$Cd_{0.93}Zn_{0.07}Te$	2.740±0.008	2038.3±13.7	3.374±0.027
$Cd_{0.89}Zn_{0.11}Te$	2.337±0.013	1868.3±2.9	2.856±0.012
$Cd_{0.5}Zn_{0.5}Te$	1.901±0.039	1794.0±10.8	2.473±0.040
$Cd_{0.1}Zn_{0.9}Te$	3.368±0.025	2600.0±17.8	4.771±0.050
$Cd_{0.04}Zn_{0.96}Te$	4.881±0.015	3301.7±29.3	7.294±0.045
ZnTe	9.071±0.043	4387.3±57.3	13.214±0.204

The thermal diffusivity and effusivity values are given as average from three independent measurements with standard deviation as uncertainty. Uncertainties of the thermal conductivity were calculated using total differential method as simply average errors taking into account thermal diffusivity and effusivity errors. The experimental reproducibility leads to the thermal conductivity uncertainty of the order of 0.5-1.5%, depending on the sample. The thickness of the specimens was measured with a micrometer with an accuracy of 10 μm, which produces additional uncertainty of about 0.2-0.3%. The systematic error connected with the presence of coupling fluid can be estimated as 3-4% [H5]. One can conclude that final uncertainty of the thermal conductivity value is of the order of 5-6%. Confirmation of

this conclusion is a comparison of the obtained thermal conductivity value of the ZnSe binary compound with the literature data. The author of the proposal obtained a value of 17.68 $W \cdot m^{-1} \cdot K^{-1}$, slightly less than the literature (19 $W \cdot m^{-1} \cdot K^{-1}$ [22]). However, taking into account the non-ideal experimental conditions as well as the influence of the growth process by various techniques, the difference is not large.

As it was described in subsection 4.1, adding manganese, zinc, magnesium or beryllium to mixed crystals results in a decrease in the value of all thermal parameters. A particularly strong decrease in thermal conductivity is observed for $Zn_{1-x}Mg_xSe$ crystals, where conductivity drops from about 18 $W \cdot m^{-1} \cdot K^{-1}$ for pure ZnSe to 2.3 $W \cdot m^{-1} \cdot K^{-1}$ for $Zn_{O.67}Mg_{0.33}Se$ compound. A similar effect is observed in case of crystals with beryllium. The decrease in transportation capacity of the mentioned compounds is due to the increasing concentration of various defects in these crystals. With the concentration of added elements in case of ternary and quaternary compounds, the quality of their crystal structure deteriorates and the disorder of the lattice increases.

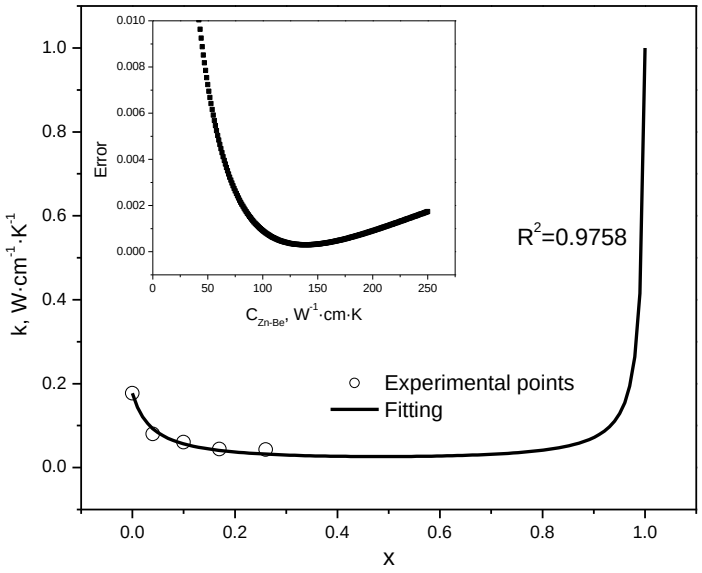

Fig. 17. Thermal conductivity *k* vs. composition *x* for $Zn_{1-x}Be_xSe$ alloy (a). The open circles represent the experimental data and solid line is best fit obtained from Eq. (23). Error arising from fitting procedure is also given in inset.

Analysis of the transport properties of the investigated compounds is not easy task due to the various effects that occur at the time of compound formation. $Zn_{1-x}Be_xSe$ crystals are a good example here. On the one hand, it is shown that as the beryllium concentration increases, the microhardness increases, on the other hand, the lattice disorder is increasing. In turn, the addition of magnesium to the ternary compound $Zn_{1-x}Be_xSe$ paradoxically improves its transport properties as it has been shown due to compensation effects that reduce the concentration of cation vacancies. This is clearly evident in the results presented in Table 4, where the resulting thermal conductivity of $Zn_{0.72}Be_{0.06}Mg_{0.22}Se$ sample is comparable to the value obtained for the $Zn_{0.74}Be_{0.26}Se$ crystal and even higher than for $Zn_{0.78}Mg_{0.22}Se$ alloy.

The electron contribution to the thermal conductivity in case of wide-gap II-VI crystals is very small indicating that the heat is mainly carried by phonons [8]. Therefore, the thermal conductivity of the crystal can be related only to the lattice contribution. In this case, the approximate formulas (22) and (23) are correct. The thermal conductivity results obtained for the ternary semiconductor crystals $Zn_{1-x}Be_xSe$, $Zn_{1-x}Mg_xSe$ and $Cd_{1-x}Zn_xTe$ were analyzed in the model given by Adachi. Fig. 17 presents the thermal conductivity *K(x)* as a function of composition at room temperature for selected $Zn_{1-x}Be_xSe$ alloys. Best fit of Eq. (23) applying least square method was obtained for following parameter values: $C_{Zn\text{-}Be}$= 139 $W^{-1}\cdot cm\cdot K$ and K_{BeSe} = 1 $W\cdot cm^{-1}\cdot K^{-1}$. Determination coefficient R^2 indicating the quality of the fitting procedure was equal 0.9758. Similar results were obtained for $Zn_{1-x}Mg_xSe$ alloy, where $C_{Zn\text{-}Mg}$= 116 $W^{-1}\cdot cm\cdot K$. Parameters $C_{Zn\text{-}Be}$ and $C_{Zn\text{-}Mg}$ describe contribution arising from the lattice disorder and are 2-6 times larger than obtained by Adachi for typical III-V ternary compounds [13]. However, the character of the change of the lattice thermal conductivity is in principal the same. One can observe rapid decrease and increase of the thermal conductivity for *x* value close to 0 and 1, respectively. Meanwhile in the middle of the graph there is plateau.

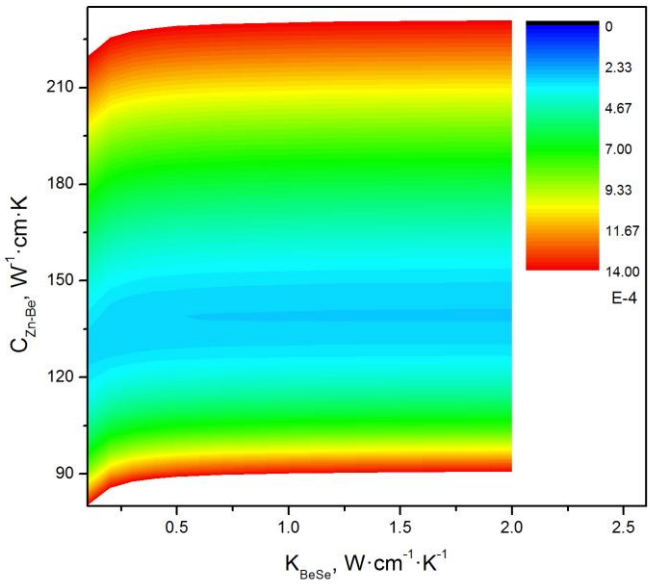

Fig. 18. Contour map of the error from two parameter ($C_{Zn\text{-}Be}$ *and* K_{BeSe}) fitting procedure with least square method.

Since the experimental data ends at *x* = 0.26 and due to the nature of the thermal conductivity change in the vicinity of *x* = 1, it is very difficult to obtain from this data the reliable thermal conductivity value of pure BeSe. This problem is illustrated in Fig. 18, in which the error resulting from the least squares procedure for the two parameters: $C_{Zn\text{-}Be}$ and k_{BeSe} is shown. While the minimum on the *y*-axis is well-located, on the *x*-axis, describing the thermal conductivity of the BeSe compound, is much stretched, making it impossible to determine the value of the k_{BeSe} parameter. The author tested the model given by Adachi for the ability to estimate the value of this parameter. It turned out that at *x* = 0.8 on the error map the minimum on the *y*-axis starts to appear. Unfortunately, the melting point of the

$Zn_{0.2}Be_{0.8}Se$ compound is beyond of our crystal growth system. In nature there are no pure BeSe or MgSe binary compounds, also it is very hard to obtain them. Accordingly, there is no experimental data describing the properties of these compounds. However, theoretical predictions regarding the expected values of such materials can be found in the literature. Theoretical calculations indicate the thermal conductivity of beryllium selenide of about 1 $W \cdot cm^{-1} \cdot K^{-1}$, and this value was used in equation (23). This value is typical rather for III-V crystals than II-VI, which confirms the atypical properties of mixed $Zn_{1-x}Be_xSe$ crystals compared to other II-VI compounds. In these crystals, the character of the bond is more covalent than that of other II-VI compounds, where the bonds are of the ionic type. As a result, these crystals are characterized by interesting properties such as small lattice constant or large energy gap.

For $Cd_{1-x}Zn_xTe$ crystals, the relationship of the thermal conductivity in the full range of compositions was obtained, i.e. from one binary compound to another (from CdTe to ZnTe) [H1]. The results analyzed in the Adachi model are shown in Figure 19.

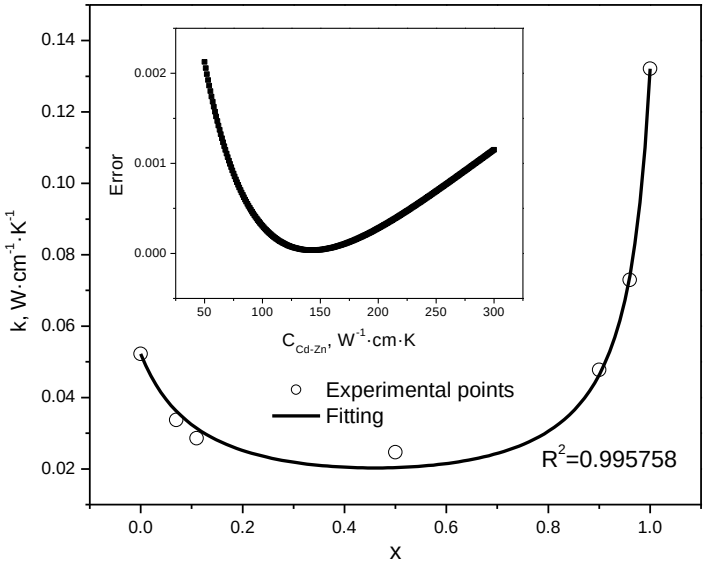

Fig. 19. Lattice thermal conductivity versus composition for $Cd_{1-x}Zn_xTe$ alloys. The points refer to the experimental data and solid line is best fit obtained using Eq. (23) applying least square method. Error arising from fitting procedure is shown in inset.

The points represent the experimental data, the line is the fit of the equation (23) with the determination coefficient R^2=0.995758. The character of the thermal conductivity changes in the function of the composition is similar to that of the $Zn_{1-x}Be_xSe$ and $Zn_{1-x}Mg_xSe$ crystals. The $C_{Cd\text{-}Zn}$ coefficient was obtained as 139 $W^{-1} \cdot cm \cdot K$, exactly the same as for the $Zn_{1-x}Be_xSe$ crystals.

In summary, as can be seen from the three groups of crystal samples, the thermal parameters are very sensitive to the change of composition, especially for the limit values of *x* lying near 0 and 1. It is possible therefore (after prior calibration) to determine the composition of newly obtained crystals from a given group by measuring their thermal properties and thanks to that also a lattice constant and energy gap.

5. Summary

The selected publication cycle presents the results of the thermal properties of a number of II-VI semiconductors. All tested crystals were grown using the high pressure Bridgman method and prepared for the research at the Institute of Physics NCU with the lead role of the author of the proposal. The measurements were carried out during the post-doctoral stay in Romania and after returning to the country on an own-built experimental setup. Informal co-operation with the Romanian center continues, as evidenced by further joint publications. The main objective of the presented work was systematic examination of selected II-VI crystals in terms of their thermal properties using various research techniques, both contact (PPE photopyroelectric) and non-contact (active thermography). As a result of the studies, the values of the thermal diffusivity and the effusivity of all tested samples were obtained. For the selected series of crystals, their heat capacity was also determined. The thermal conductivity was calculated using simple relationships that combine all the thermal parameters. In this way a complete characterization of the thermal properties of the crystals was carried out and the main purpose of the work was realized.

The first results obtained for binary, $Cd_{1-x-y}Zn_xMg_ySe$ and $Zn_{1-x-y}Be_xMn_ySe$ crystals were reported in H2, H4 and H8 respectively. At this stage, the crystals were examined both using PPE (BPPE and TWRC) contact methods as well as by non-contact active thermography. The highest thermal conductivity values were observed for binary and mixed crystals with low concentration of added component. Adding even a few atomic percent of the foreign cation to any mixed crystal immediately caused a significant deterioration in its thermal properties. The thermal conductivity values differed between the binary ZnSe compound and the mixed crystals $Cd_{1-x-y}Zn_xMg_ySe$ or $Zn_{1-x-y}Be_xMn_ySe$ even by the order of magnitude. The addition of manganese, beryllium or magnesium generated significant concentrations of various defects in these compounds, and as a consequence the thermal transport parameters of such crystals have been substantially reduced. Due to the problem of heat dissipation in electronic devices, this observation is crucial in the process of designing new optoelectronic devices based on any mixed compounds.

Particularly important were the results obtained for binary crystals and glassy carbon (GC) samples, as the experimental values were comparable to the literature data. The final results of the thermal conductivity in case of binary crystals deviated from the literature data. The differences between the values obtained and the literature data observed in this case were explained by the effect of the non-ideal blackening layer or/and by the presence of a coupling liquid in the sample/detector system. The thermal conductivity values obtained for the GC reference sample matched the literature data. On the other hand, while comparing literature data on the thermal diffusivity and effusivity of the GC, they were appropriately understated and overvalued.

Observed discrepancies between the literature and measured data prompted the author to look more closely at the used measurement techniques, resulting in two more co-author publications (H3 and H5). It has been known from other authors that the main problem with PPE technique is the effect of the coupling layer, which always influences obtained results. The question was how great the problem is in this particular case, i.e. for the tested material class. In order to analyze this problem, various coupling fluids commonly used in

photopyroelectric techniques have been tested first. As the most optimal, i.e. giving the least underestimation, ethylene glycol was chosen which was used in the course of further research. In order to analyze the quantitative influence of the coupling layer on the obtained thermal diffusivity value, simulations were carried out based on a five-layer theoretical model. The results clearly showed that the critical factor in BPPE contact measurement is the thickness of the coupling layer. This effect is further enhanced for high-conductivity samples. In order to minimize the impact of the ethylene glycol layer, a simple modification to the standard measuring system was introduced. The modification consisted of pressing the test sample to the detector by means of a disk and three identical actuating springs, thereby reducing the thickness of the coupling layer. The results obtained with the modified system allowed further reducing of the underestimation to the value of 3-4% of the measured value.

In the case of non-contact active infrared thermography, it turned out that the received thermal diffusivity values are sensitive to the geometry of the measuring system. In the case of inaccurate sample setting with respect to the camera, the slopes obtained from the phase profiles differ from each other, generating a relatively high measurement uncertainty of up to a few percent of the measured value. In addition, the measured samples should be thermally thick. Failure to do so results in an underestimation of thermal diffusivity of up to 20-30%. Choosing the right frequency is therefore critical, but it is not an easy task in case of new materials with unknown thermal parameters. For new materials to determine the approximate frequency of modulation, one can use the contact photopyroelectric method first.

As a result of the optimization processes, the thermal diffusivity values of the reference materials according to the literature data were obtained. The results presented in the last three publications (H1, H6, H7) were obtained taking into account the conclusions obtained from the optimization of the measurement methods. The thermal diffusivity measurements of the crystals were made using a modified measuring system and ethylene glycol as the coupling liquid between the sample and detector. In addition, as in the TWRC method it is difficult to determine the accuracy of the obtained results and due to the degree of complexity of the experiment, the results of the thermal effusivity measurements were obtained in the FPPE configuration. The total uncertainty of the thermal conductivity of the examined crystals was estimated at 5-6% of the measured value. Confirmation of this conclusion was a comparison of the obtained thermal conductivity value of the ZnSe binary compound with the literature data. As with previous crystals, the addition of manganese, zinc, magnesium or beryllium to mixed crystals resulted in a decrease in the value of all thermal parameters. A particularly strong decrease in thermal conductivity was observed for $Zn_{1-x}Mg_xSe$ crystals, where the conductivity decreased from about 18 $W \cdot m^{-1} \cdot K^{-1}$ for pure ZnSe to 2.3 $W \cdot m^{-1} \cdot K^{-1}$ for $Zn_{O.67}Mg_{0.33}Se$ compound. Similar effects have also been observed for crystals with beryllium. The thermal conductivity results obtained for the ternary semiconductor crystals $Zn_{1-x}Be_xSe$, $Zn_{1-x}Mg_xSe$ and $Cd_{1-x}Zn_xTe$ were analyzed in a model provided by Adachi. The C_{Zn-Be}, C_{Zn-Mg} and C_{Cd-Zn} parameters (139, 116 and 139 $W^{-1} \cdot cm \cdot K$ respectively) describing the contribution to thermal resistance resulting from the lattice disorder were 2-6 times higher than those obtained by Adachi for III-V semiconductors. However, the character of the change of the thermal conductivity in the function of the composition was the same for both classes of materials.

Although the PPE technique itself is fairly simple, each material class requires a different approach. For samples with strongly different conductivity or thickness, different frequency ranges and a suitable detector should be used. This is not a simple task for the samples with unknown thermal properties. However, the results presented in this proposal indicate that the set objectives have been met. The photopyroelectric technique has been successfully adopted for the study of the given material class. This has led to more than two hundred II-VI semiconductor samples being characterized for thermal properties. The direct results of the disorder as the function of the composition for selected groups of ternary crystals were also presented.

All measurements made within this work were carried out at room temperature. In the longer term, measurements are planned as a function of temperature. For this purpose, a suitable measuring cell was designed and constructed which can be placed on a helium cryostat finger. This will allow performing measurements from temperatures of the order of 10 K to about 400 K. The first test measurements are currently in progress.

In the presented publication cycle, optically opaque samples were examined using only one wavelength of the excitation radiation. In the same measuring system, however, it is possible to excite the sample with variable wavelength. This will allow determining the absorption coefficient as a function of the wavelength, energy gap and the thermal diffusivity of the sample in one measurement. For this purpose, a program for spectral measurements using PPE method and impulse laser combined with OPO (parametric oscillator) was designed and created. Compared to classical spectral techniques such as transmission, PPE spectroscopy can test samples with very high absorption coefficient values. In the case of II-VI materials, the absorption coefficient above the energy gap may reach thousands of inverted centimeters. These further work perspectives are the result of the presented publication cycle and should contribute to a further increase in the knowledge of the properties of the studied materials.

Literature

[1] A.P. Ravikumar, T.A. Garcia, J. de Jesus, M. Tamargo, C. Gmachl, Appl. Phys. Lett.105 (2014) 061113.

[2] P. Wojnar, E. Janik, L.T. Baczewski, S. Kret, E. Dynowska, T. Wojciechowski, J. Suffczynski, J. Papierska, P. Kossacki, G. Karczewski, J. Kossut, T. Wojtowicz, Nano Lett. 12 (7) (2012) 3404.

[3] A. Shen, A.P. Ravikumar, G. Chen, K. Zhao, A. Alfaro-Martinez, T. Garcia, J. de Jesus, M.C. Tamargo, C. Gmachl, J. Vac. Sci. Technol. B 31 (2013) 03C113.

[4] Y.N. Hou, Z.X. Mei, H.L. Liang, D.Q. Ye, C.Z. Gu1, X.L. Du, Appl. Phys. Lett. 102 (2013) 153510.

[5] M. Niraula, K. Yasuda, H. Yamashita, Y. Wajima, Y. Tsukamoto, M. Matsumoto, Y. Suzuki, N. Takai, Y. Tsukamoto, Y. Agata, Phys. Status Solidi C 11 (2014) 1333.

[6] K.M. Yu, M.A. Mayer, D.T. Speaks, H. He, R. Zhao, J. Appl. Phys. 111 (2012) 123505.

[7] L. Xiao, D. Mei, M. Cao, D. Qu, B. Deng, J. Alloy. Compd. 627 (2015) 455.

[8] G. Slack, Phys. Rev. B 6 (1972) 3791.

[9] A. Mandelis, M.M. Zver, J. Appl. Phys. 57 (1985) 4421.
[10] M. Chirtoc, G. Mihailescu, Phys. Rev. B 40 (1989) 9606.
[11] D. Dadarlat, Laser Phys. 19 (2009) 1330.
[12] B. Abeles, Phys. Rev. 131 (1963) 1906.
[13] S. Adachi, J. Appl. Phys. 54 (1983) 1844.
[14] M. Marinelli, F. Mercuri, U. Zammit, R. Pizzoferrato, Appl. Phys. A 52 (1991) 115.
[15] A. Salazar, Rev. Sci. Instrum. 74 (2003) 825–827.
[16] A. Salazar, Oleaga, Rev. Sci. Instrum. 83 (2012) 014903.
[17] C. Boue, S. Hole, Infrared Phys. Technol. 55 (2012) 376.
[18] J. Shen, A. Mandelis, Rev. Sci. Instrum. 66 (1995) 4999.
[19] H.W. Carslaw, J.C. Jaeger, Conduction of heat in solids. 2nd ed. London, UK: Oxford Univ. Press, (1959).
[20] F. Firszt S. Łegowski, H. Meczynska, J. Szatkowski, W. Paszkowicz and K. Godwod, J. Cryst. Growth 184/185 (1998) 1335.
[21] D. Dadarlat, M. Streza, M.N. Pop, V. Tosa, S. Delenclos, S. Longuemart, A.H. Sahraoui, J. Therm. Anal. Calorim. 101 (2010) 397.
[22] O. Madelung, Semiconductors: data handbook, Berlin: SpringerVerlag (2003).
[23] http://www.htw-gmbh.de/, dostęp 15 Maja 2017.
[24] M. Pawlak, F. Firszt, S. Łęgowski, H. Męczyńska, J. Gibkes, J. Pelzl, Int. J. Thermophys. 31 (2010) 187.
[25] M. Chirtoc, C. Glorieux, J. Thoen, in: E.M. Moares (Ed.), Thermal Wave Physics and Related Photothermal Techniques: Basic Principles and Recent Developments, Transworld Research Network, Trivandrum, Kerala, India, (2009) 125.
[26] H. Coufal, A. Mandelis, Ferroelectrics 118 (1991) 379.
[27] http://www.sttic.com.ru/, dostęp 15 Maja 2017.

Karol Strzałkowski

5. Discussion of the other scientific (artistic) accomplishments.

Since 2003 I have worked as a researcher at the Department of Semiconductor and Carbon Physics of Institute of Physics NCU dealing with preparation and study of photothermal, photoelectric and luminescent properties of broadband ternary and quaternary II-VI compounds with manganese and beryllium as ingredients. Doctoral thesis entitled "Synthesis and study of photothermal and photoelectric properties of mixed AII - BVI crystals" I have defended and got a PhD in physical sciences 24th June 2008.

At the Department of Semiconductor and Carbon Physics crystals are grown from the melt under overpressure (approx. 130-150 atmospheres) of argon. This method is technologically difficult and requires high accuracy and responsibility. I am currently one of two people of the group who work on the synthesis of mixed II-VI crystals. In addition to standard spectroscopic techniques (photoluminescence, transmission) I have also mastered at this time measurements of the photothermal properties of obtained semiconductor compounds using the photoacoustic methods with piezoelectric, microphone and pyroelectric detection

and I have in this field practical experience. The main objectives of the research consisted of growing of series of mixed II-VI crystals based on ZnSe, CdSe with beryllium, magnesium and manganese as constituents, and their characterization with optical spectroscopy and photoacoustic techniques.

After the measurements of lots of photoacoustic spectra of different II-VI crystals it was noted that the shapes of the obtained spectra, both in the phase and in the amplitude, measured for the same type of crystal, often markedly were different from one another. In search for reasons of this observation it was highlighted that in these cases the surfaces of the test samples were prepared in different ways. The study focused then on investigation of the effect of the surface condition on the measured photoacoustic characteristics. We have been studied the effect of mechanical surface preparation (grinding, polishing and chemical etching [1]) and the influence of the polarity of the crystal surface on obtained photoacoustic spectra. The measurements were conducted after a surface treatment procedure for the samples of the same type (ground, polished, chemically etched and annealed in cation vapor). Such studies have been performed for $Zn_{1-x-y}Be_xMg_ySe$ [2,3] and $Zn_{1-x-y}Be_xMn_ySe$ [4-6] compounds both in the rear and front configuration, as well. The measurements were performed at each stage of the surface processing. Photoacoustic spectroscopy has proved to be very sensitive to the processes, which investigated crystals were subjected to. The absorption bands within bandgap of investigated compounds have been identified and connected with localized defects on a sample surface. In case of $Zn_{1-x-y}Be_xMg_ySe$ compound the samples were excited successively from both sides. Obtained results suggested a slightly different distribution of individual defects on each side. Such assumptions helped achieve a satisfactory fit of the experimental results in frame of a theoretical model proposed by Maliński. The samples used for testing were not oriented along any crystallographic plane.

After PhD further measurements were carried out with the aim of developing and verification of the Maliński model. The research was made on ZnSe samples, oriented and cut along the specific chosen crystallographic planes [7]. We have also successfully correlated qualitatively the results obtained for $Zn_{1-x-y}Be_xMn_ySe$ crystals with photoacoustic detection and from atomic force microscope (AFM). AFM microscopy allowed examining the topography of the surface of the samples subjected to different technological processes of surface treatment [8].

Using photoacoustic frequency characteristics we have determined a very important material parameter of $Zn_{1-x-y}Be_xMn_ySe$ crystals which is the thermal diffusivity. In order to determine this parameter the theory developed by Blonskij and co-workers has been used, which is a special modification of the Jackson and Amer theory. The results indicated an increase of the thermal diffusivity with increasing content of beryllium, magnesium and manganese in the crystals. However, we could not determine clear dependence of the thermal diffusivity on the composition. This could be due to the fact that the obtained values were subjected to considerable measurement error. The biggest influence on the thermal diffusivity has a content of beryllium. Manganese also to some extent increases the value of the thermal diffusivity of the tested crystals. On the other hand, large concentrations of Be, as well as Mn, are causing in the crystal generation of various defects. These defects may act as scattering centers for phonons, resulting in a brake of further increase of the thermal diffusivity of the crystal and may even lead to the decrease. In summary, thermal diffusivity values obtained

using the piezoelectric method proved to be very inaccurate, which was one of the reasons of my interest after PhD of pyroelectric detection.

Photoluminescence spectra of the investigated II-VI compounds consisted of exciton line, edge emission and the bands associated with deep levels. The relative contribution of the entire measured spectrum (and the position) of the individual luminescence components were different for the different compounds. Additionally, in the photoluminescence spectrum of $Zn_{1-x-y}Be_xMn_ySe$ crystals an intensive manganese emission with a maximum corresponding to the energy of about 2 eV has been observed. For crystals with a high content of manganese it was the only luminescence observed in the range of 30K to room temperature. In case of the mixed $Zn_{1-x-y}Be_xMn_ySe$ crystals anomalous shift of the maximum of manganese emission depending on the temperature has been observed. With increasing temperature maximum of the emission shifted first towards lower energies and then in the opposite direction. This effect was explained by a negative temperature expansion of the crystals lattice. For crystals with constant manganese content at constant temperature the emission shifted monotonically towards lower energies with increasing beryllium concentration. This observation was caused by a change of the ionic bond to more covalent and decreasing of the lattice constant, which influenced the crystal field value seen by the manganese ions [10]. During further study (after PhD) the shift of the manganese emission also with the excitation radiation power [11] has been found.

The band gap of the investigated compounds ($Zn_{1-x-y}Be_xCd_ySe$, $Zn_{1-x-y}Be_xMg_ySe$ and $Zn_{1-x-y}Be_xMn_ySe$) increased with increasing zinc, magnesium and beryllium concentration. On the other hand, for manganese content (from y = 0.05 and y = 0.2) in case of $Zn_{1-x-y}Be_xMn_ySe$ only small change of the energy gap was observed [9-11]. The values of exciton energy gap determined from photoluminescence were clearly lower than obtained from photoacoustics, which is understandable, because the exciton binding energy in II-VI crystals is of the order of tens of meV. This observation was the basis of the developing (after PhD) of the method of the determining of the binding energy of the excitons [12] in II-VI materials. In the case of crystals with manganese, excitonic emission was not observed at higher temperatures. For the $Zn_{0.9}Be_{0.05}Mn_{0.05}Se$ crystal the exciton position as the function of the temperature was found in the range of 30 K to 210 K. For the other crystals excitonic line was visible at low temperatures, and for the two compounds, $Zn_{0.7}Be_{0.1}Mn_{0.2}Se$ and $Zn_{0.78}Be_{0.15}Mn_{0.07}Se$, it was not observed even at 35 K. In case of the crystals in which the exciton was observed at low temperature, E_{gex} was estimated at room temperature using a difference between the position of the exciton line at 30K and at room temperature obtained for $Zn_{0.9}Be_{0.05}Mn_{0.05}Se$ compound. The energy gap of the crystals, in which the exciton was not observed even at low temperatures was determined at room temperature by photoacoustic spectroscopy.

Photoconductivity spectra of $Zn_{1-x-y}Be_xMn_ySe$ compounds were also studied. It was found that the measured spectra did not show a significant correlation with the photoacoustic spectra, but were also not opposed to them. The observed bands in the spectrum of photoconductivity were wide and overlapping each other. Theoretically it was possible to obtain the E_g value from this measurement, but the obtained results would be unreliable.

Exciton line widths at 30 K of all tested ternary and quaternary compounds were larger than in the case of a binary ZnSe. The reason is the chemical disorder, with which we are dealing in these compounds. The confirmation of the existence of a chemical disorder was

also found in transmission spectra of these compounds by observation of the blurring of the absorption edge near energy gap value. The behavior of the transmission in the case of the quaternary crystal is different than in binary ZnSe. In case of ZnSe crystal the transmission changes from 90% to zero in a narrow energy range (typically less than 0.05 eV), on the other hand for quaternary compounds, the present range is much larger and is of the order of several tenths of eV. The manganese ions in the $Zn_{1-x-y}Be_xMn_ySe$ crystals lead to the presence in these compounds of strong absorption bands in the region below the energy gap. For this reason it was not possible to determine the value of the energy gap from transmission in such case. Chemical disorder effects made also difficult determination of the energy gap from photoacoustic measurements. The biggest disorder effects were observed in case of $Zn_{1-x-y}Be_xCd_ySe$ compounds. In these crystals E_{gfa} values were obtained with high uncertainty. For the other two compounds, namely $Zn_{1-x-y}Be_xMg_ySe$ and $Zn_{1-x-y}Be_xMn_ySe$, observed blurring of fundamental absorption bands were much smaller, and consequently the estimated error was significantly lower than in case of the crystals with cadmium. Using the photoacoustic amplitude spectra the calculations of the absorption coefficient as the function of the energy was carried out. However, one could not find a straight line on the graph $(\alpha h\nu)^2$ vs. energy, which determines the value of the energy gap. One reason for this was undoubtedly the aforementioned blurring of the band edges, caused by a chemical disorder.

In the case of measurements of photoluminescence excitation spectra and absorbance of $Zn_{1-x-y}Be_xMn_ySe$ crystals transition which take place inside the manganese ion from the ground state to the excited states have been found and identified [9-11]. Similar absorption bands were also observed in the photoacoustic spectra. The obtained values were in good agreement with literature data for the case of the excited states of manganese ion in a tetrahedral crystal field. Photoluminescence measurements of $Zn_{1-x-y}Be_xMn_ySe$ crystals were also carried out at a characteristic excitation (at the maxima of the absorption bands of manganese). Spectra obtained at 250 K at an excitation wavelength of 540 nm showed two maxima. This was probably due to the fact that radiation having a wavelength of 540 nm was in a range that caused a characteristic energy excitation of other band (with non-manganese origin), such as it is in the case of ZnSe.

After PhD measurements of selected compounds using microphone detection have been performed. For this purpose open photoacoustic cell with a microphone as a detector was designed and made. The measurements of zinc selenide sample with a small amount of cobalt [13] allowed to determine the value of its energy gap, the position of cobalt absorption bands and the estimation of the quantum yield (in infrared region) at room temperature. Similar measurements were also carried out for $Zn_{1-x-y}Be_xMn_ySe$ crystals with manganese [14].

Literature

[1] M. Maliński, J. Zakrzewski, K. Strzałkowski, *Evaluation of the quality of the etching process with the piezoelectric spectroscopy method*, J. Phys. Conf. Ser. 214 (2010) 012069.

[2] M. Maliński, J. Zakrzewski, K. Strzałkowski, S. Łęgowski, *Photoacoustic Spectroscopy of ZnBeMgSe Mixed Crystals*, Acta Acust. United Acust. 94 (2008) 250-253.

[3] M. Malinski, J. Zakrzewski, K. Strzałkowski, S. Łegowski, F. Firszt, H. Meczynska, *Piezoelectric photoacoustic spectroscopy of surface states of Zn0.81Be0.04Mg0.15Se*

mixed crystals, Surf. Sci. 603 (2009) 131-137.
[4] M. Maliński, J. Zakrzewski, and K. Strzałkowski, *Numerical Analysis of Piezoelectric Spectra of Zn1-x-yBexMnySe Mixed Crystals*, Int. J. Thermophys. 28 (2007) 299-316.
[5] J. Zakrzewski, M. Maliński, K. Strzałkowski, F. Firszt, S. Łęgowski, H. Męczyńska and A. Marasek, *Study of Zn1-x-yBexMnySe mixed crystals by photothermal method*, Eur. Phys. J. Special Topics 153 (2008) 267-270.
[6] J. Zakrzewski, M. Maliński, K. Strzałkowski, F. Firszt, S. Łęgowski, H. Męczyńska, *Piezoelectric spectroscopic studies of Zn1-x-yBexMnySe mixed crystals*, Eur. Phys. J. Special Topics 154 (2008) 381-385.
[7] J. Zakrzewski, Mirosław Maliński, K. Strzałkowski, *Influence of the Surface Mechanical Treatment on the Photothermal Piezoelectric Spectra of ZnSe Crystals*, Int. J. Thermophys. 33 (2012) 1228 - 1238.
[8] K. Strzałkowski, S. Kulesza, J. Zakrzewski, M. Maliński, *Surface investigations of ZnBeMnSe mixed crystals by means of the piezoelectric spectroscopy and the AFM technique*, Appl. Surf. Sci. 290 (2014) 27 – 34.
[9] F. Firszt, K. Strzałkowski, J. Zakrzewski, S. Łegowski, H. Męczyńska, M. Malinski, D. O. Dumcenco, C. T. Huang, Y. S. Huang, *Optical and photothermal investigations of Zn1-x-yBexMnySe solid solutions*, Phys. Stat. Sol. B 247 (2010) 1402-1404.
[10] F. Firszt, K. Strzałkowski, J. Zakrzewski, S. Łęgowski, H. Męczyńska, and A. Marasek, *Photoelectric and photothermal investigations of Zn1-x-yBexMnySe solid solutions*, Cryst. Res. Technol. 42 (2007) 1352-1358.
[11] K. Strzałkowski, F. Firszt, A. Marasek, *Photoluminescence of ZnBeMnSe solid solutions*, J. Lumin. 184 (2017) 29 – 37.
[12] K. Strzałkowski, J. Zakrzewski, M. Maliński, *Determination of the Exciton Binding Energy Using Photothermal and Photoluminescence Spectroscopy*, Int. J. Thermophys. 34 (2013) 691 – 700.
[13] Łukasz Chrobak, M. Maliński, K. Strzałkowski, J. Zakrzewski, *Energy efficiency of near infrared cobalt luminscence in ZnSe:Co determined by a photoacoustic method*, Opto-Electron. Rev. 20(1) (2012) 91 - 95.
[14] Ł. Chrobak, M. Maliński, J. Zakrzewski, K. Strzałkowski, *Photoacoustic method of determination of quantum efficiency of luminescence in Mn 2+ ions in Zn1–x–yBexMnySe crystals*, Opto-Electron. Rev. 19(2) (2011) 183 - 188.